



INVESTIGATION OF STRESSES
IN THE
ALGOL II-B ROCKET NOZZLE MODEL

Herbert Becker
C. N. Tang

Final Technical Report ARA 297-1
25 February 1966

Prepared for

Contract No. NAS1-5191
Langley Research Center,
Langley Station,
Hampton, Virginia.

ALLIED RESEARCH ASSOCIATES, INC.
VIRGINIA ROAD • CONCORD, MASSACHUSETTS

ABSTRACT

23460

A three-dimensional photoelastic model of the Algol II-B solid propellant rocket motor nozzle constructed under a previous NASA contract (NAS1-3975) was modified and instrumented for testing at higher applied pressures and under thermal gradients. A computer analysis was performed by the Aerojet General Corporation for both pressure and thermal loading for comparison with the results of these tests. In addition, two dimensional beam-on-elastic-foundation models were constructed and tested.

Generally good agreement was obtained between theoretical results and test results, confirming the low stress levels reported by ARA in NASA CR 66026 (final report on Contract NAS1-3975). The two dimensional beam-on-elastic-foundation model was demonstrated to be applicable to axisymmetric shell analysis.

Auth

SUMMARY

In this culmination of the Algol Rocket Nozzle investigation, the previously constructed 3-dimensional photoelastic model of the II-B nozzle was modified and instrumented for testing at higher pressures than previously, and for thermoelastic analysis. A computer analysis was performed by the Aerojet General Corporation for comparison with the results of those experiments. In addition, beam-on-elastic-foundation 2-dimensional models were constructed and tested.

The results showed generally good agreement, confirming the low stress levels reported previously by ARA in the initial experimental program. In addition, the 2-dimensional beam-on-elastic-foundation model was demonstrated to be applicable to axisymmetric shell analysis.

TABLE OF CONTENTS

	<u>Page</u>
SUMMARY	ii
SYMBOLS	v
1. INTRODUCTION	1
2. THREE DIMENSIONAL INVESTIGATION	2
2.1 Experimental Program	2
A. Introduction	2
B. Model Modifications	2
C. Recording Equipment	6
D. Pressurization System	6
E. Thermoelastic Arrangement	6
2.2 Experimental Data	7
A. Pressure	7
B. Temperature	9
2.3 Theoretical Analysis	15
A. Introduction	15
B. Pressure	15
C. Temperature	20
2.4 Comparison of Theory and Experiment	24
A. Pressure	24
B. Temperature	24
C. Pure Moment Loading	27
D. Summary	27
3. ELASTIC FOUNDATION MODEL STUDY	28
3.1 Introduction	28
3.2 Preliminary Studies	29
A. Purpose	29
B. Theory	29
C. Experimental Procedure	29
D. Comparison of Theory and Experiment	31
3.3 Algol II-B Simulation	38
A. Model Design	38
B. Experimental Procedure	38
C. Summary	42

TABLE OF CONTENTS (Cont'd)

4	CONCLUSIONS	45
	A. 3D Nozzle Analysis	45
	B. 2D Elastic Foundation Model	45
5	REFERENCES	46
6	APPENDIX	47
	Reproduction of AGC Summary Report on Computer Program	

SYMBOLS

A	Area of elastic foundation strut, in ²
E	Young's modulus, psi (or Msi = 10 ⁶ psi)
f	Material fringe value, psi-in/fringe
h	Depth of beam or local thickness of shell, in.
L	Length of elastic foundation strut, in.
M	Bending moment, in-lb/in.
n	Fringe order
P	Force on elastic foundation strut, lb.
p	Pressure loading on nozzle, psi
\bar{p}	Equivalent elastic foundation pressure, psi
(p - q)	Principal stress difference, psi
R	Radius of shell, in.
t	Thickness of model or bonded polariscope, in.
t ₁ , t ₂	Thicknesses of beam and elastic foundation strut, in.
V	Shear, lb/in.
W ₁ , W ₂	Widths of beam and of elastic foundation strut, in.
w	Radial motion of shell, in.
x	Axial coordinate, in.
ν	Poisson's ratio
σ	Stress, psi
σ _θ	Circumferential stress, psi
σ _r	Radial stress, psi
σ _l	Longitudinal stress, psi

1. INTRODUCTION

The basic purpose of this project initially was to evaluate photoelastically the structural performance of the Algol II-A and Algol II-B rocket nozzles. In that investigation (Ref. 1) pressure stresses were found experimentally to be only about 4 percent of those reported in a theoretical analysis (Ref. 2).

The low pressures employed in Ref. 1 to avoid model failure yielded such low fringe orders that accurate photoelastic data were difficult to obtain in the special bonded polariscopes utilized in the 3D model which was fabricated and tested. In addition, only fringe pattern data in the photoelastic plastic (representative of the refracil, carbon and fiberglass of the prototype) were obtained. No data were acquired directly on the magnesium (representative of the steel reinforcement on the prototype).

This second phase of the nozzle study was conducted to obtain data of increased accuracy by application of higher model pressure (at possible risk of failure) and to supplement the photoelastic data with strain gage data on the magnesium reinforcement, and to perform a thermal stress test in addition to the pressure test. In addition, a subcontract was let to Aerojet General to conduct computer analyses of the nozzle for both pressure and temperature loadings employing the new program developed by Wilson (Ref. 3), in order to obtain a better correlation of theory with experiment, since Ref. 3 is considered capable of representing the nozzle behavior with considerably greater accuracy than Ref. 2. In this case, however, there was a slight change of emphasis. The 3-dimensional model was the reference article instead of the prototype nozzle. The Aerojet analyses were conducted for the model geometry and materials instead of for the II-B nozzle. The results of both theoretical and experimental investigations were pertinent to the prototype, however, since the model was a closely scaled simulation of the prototype.

This second phase contained an additional feature. Preliminary efforts by ARA indicated the utility of the beam-on-elastic-foundation concept in a 2-dimensional photoelastic model to investigate the pressure stresses in the nozzle. This procedure has the potential of a simple, rapid modeling procedure which would reveal stresses more effectively than a 3-dimensional model because of the greater accessibility of the fringe patterns both in the 2D cross-section and circumferentially.

2. THREE DIMENSIONAL INVESTIGATION

2.1 Experimental Program

A. Introduction

In order to prepare the model for the current investigation, it was necessary to alter the configuration, to apply strain gages and thermocouples, and to prepare proper recording devices to accept the data. A pressurization system, a model support, and a tank for thermoelastic analysis were designed and constructed. Pressure and thermoelastic tests were conducted in which photoelastic and strain gage data yielded information on model stresses while the thermocouples in the thermoelastic tests provided the basic information for the theoretical analysis as well as for correlation with the observed stresses in the 3 dimensional model. The details of these procedures are reported in this section of the report.

B. Model Modifications

The 3 dimensional photoelastic model which was employed in the previous investigation is shown in Fig. 35 of Ref. 1. In order to convert the model to the proper geometry for the current investigation, in which the proper representation of the prototype pressure test was desired, the plexiglas throat cylinder was removed and a repair ring was cemented into the throat to yield the contour shown in Fig. 1.

Type A7 strain gages were cemented to the magnesium reinforcement in the inlet region at the locations shown in Fig. 2. These 4 gages provided strain data at the two longitudinal locations shown to permit determination of reinforcement stresses both longitudinally and circumferentially at positions of previously reported high stresses according to the theoretical analysis of Ref. 2.

Because of the radial gradients anticipated in the model during thermal transients, a careful program of investigation was conducted to determine the amount of piping of temperature to be expected with radially inserted thermocouples. These studies revealed the advisability of contouring the wires near the beads along circumferential lines for at least 1/4 in. As a result, the thermocouples were first cemented into epoxy plugs, which were then cemented into cored holes in the model at the locations shown in Fig. 3.

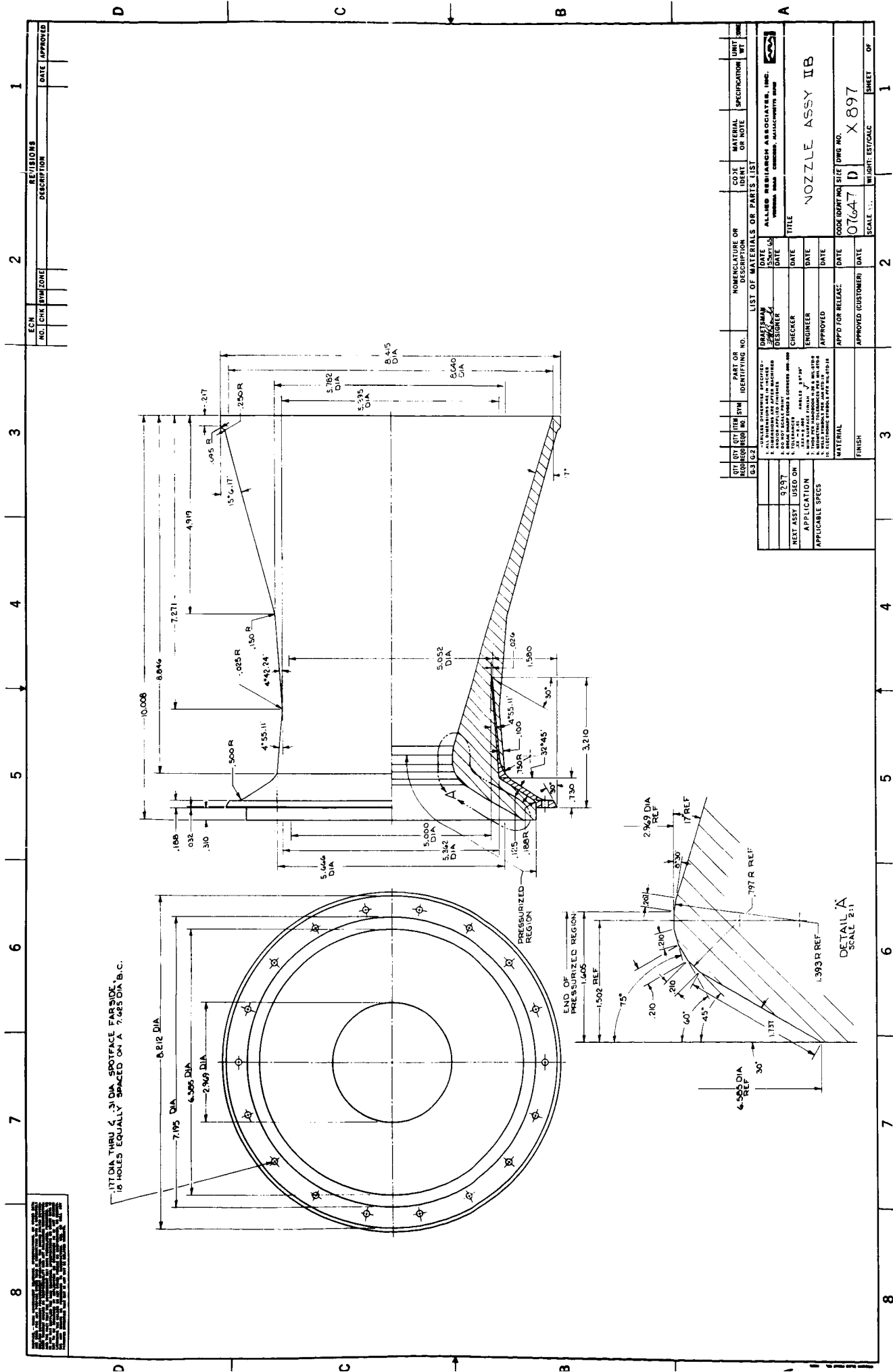


Figure 1 Modified Nozzle Geometry Showing Pressurized Region (A)

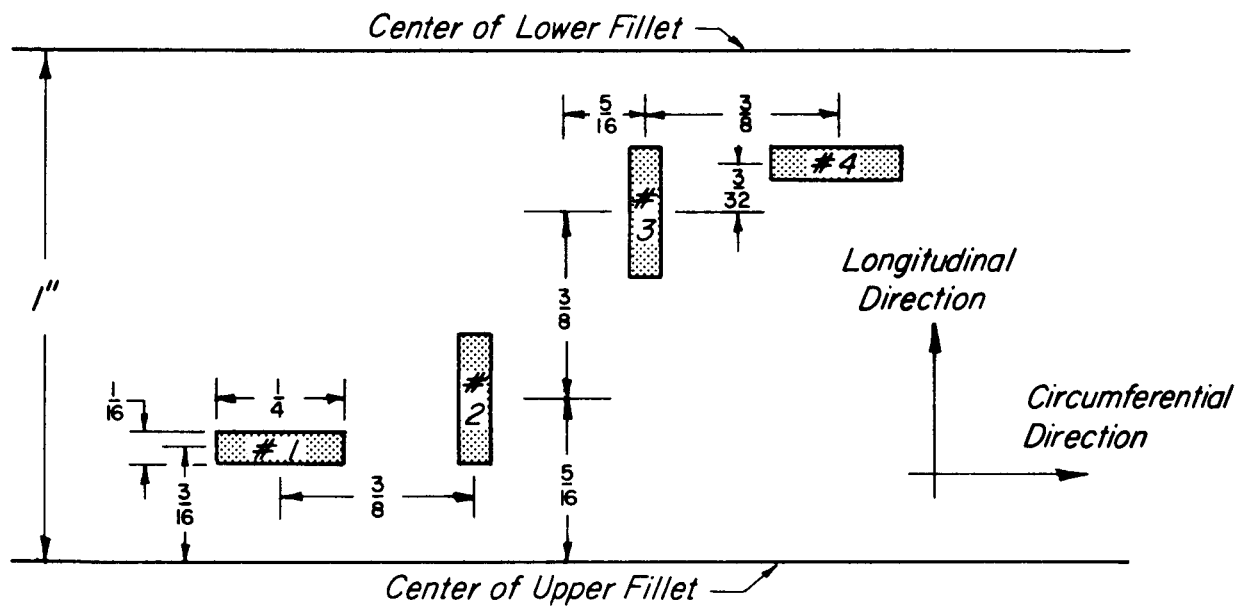


Figure 2 Strain Gage Locations

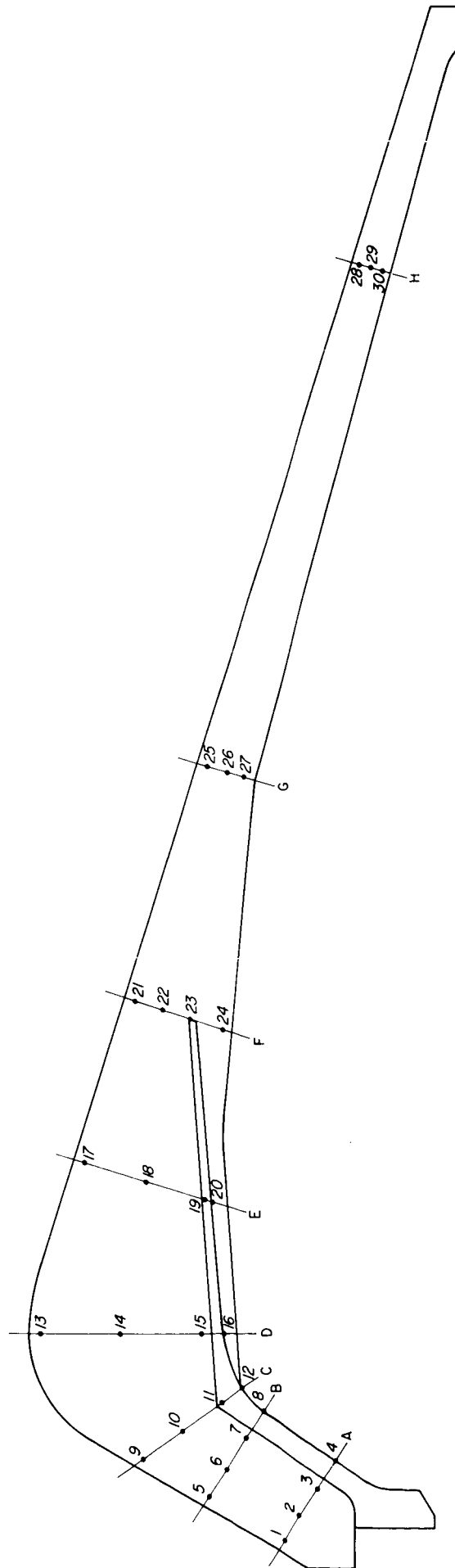


Figure 3 Thermocouple Locations

C. Recording Equipment

The thermocouple data were referred to an ice junction. The outputs were amplified with a Kintel amplifier and were recorded on a Heiland Corp. Model 708C Oscillograph. Because of the need for reliable switching to obtain the thermocouple data, extensive development was necessary to achieve effective operation of this equipment.

The strain gages were compensated by gages on magnesium blocks near the model. They were excited by 4 volts input and the output was acquired on a 4 channel Sanborn recorder.

D. Pressurization System

The pressure was applied to the model in the inlet and throat by closing the inlet with a plexiglas cover attached to the bolt circle, inserting a plunger to the center of the throat region from below, and introducing nitrogen gas in the chamber so formed.

Although polariscopes were bonded into the model (Fig. 36 of Ref. 1) to reveal stresses longitudinally throughout the inlet and throat regions, only the longitudinal polariscope nearest the inlet was visually accessible. Furthermore, difficulties in illumination made photography of the fringes at that location impossible. The throat circumferential polariscope could be photographed.

E. Thermoelastic Arrangement

The thermoelastic investigation was conducted by closing the bottom (exit) of the expansion cone and depositing chilled halowax and glycerin into the model to a level slightly above the top of the inlet surface by aid of a dam ring. The longitudinal polariscopes were inaccessible in this investigation. Fringe orders were observed visually. Complete temperature runs were recorded at intervals.

It was decided to select the temperature data for 6 minutes after introduction of the chilling fluid as the basis for the theoretical computer study to be conducted by AGC, since the maximum accuracy would be available in the photoelastic data for comparison, because at that time relatively slow changes occurred and the highest fringe orders were observed, in the circumferential polariscopes.

In addition to observing the circumferential polariscopes, thermoelastic photographs were taken of the fringes in the skirt polariscope, the results of which also were compared to the predictions of the AGC analysis.

2.2 Experimental Data

A. Pressure

The 3D model was loaded in 50 psi increments up to 200 psi. The summary of the visually observed fringe pattern data in the longitudinal polariscope appears in Table 1.

Table 1 Fringe Data from Visual Observations of Longitudinal Polariscope During 3D Pressure Test

Pressure(psi)	Inner Fringe Order	Outer Fringe Order
50	Uncertain	Uncertain
100	0.4 to 0.5	0.3 to 0.4
150	0.8	0.6
200	1	0.8

The strain gage data (Fig. 4) were converted into σ/p by using the slopes of the straight lines which were faired through the data points. The stresses were found using Hooke's Law with $E = 6.5 \text{ Msi}$ and $\nu = 0.3$. The values of σ/p are shown in Table 2 for the strain gage locations shown in Fig. 2.

Table 2 Experimental Stresses on the Surface of the Magnesium Alloy Reinforcement

Strain Gage Pair	Circumferential σ_{θ}/p	Longitudinal σ_{ℓ}/p
(1, 2)	10	25
(3, 4)	34	44

Local stress concentrations could not be discerned with certainty, although there was indication of a higher fringe order at 200 psi near the extreme outer corner in location A of Fig. 1. The difficulties in obtaining these data are charged to problems in lighting the embedded polariscope in the metal reinforcement region, and to degradation of the internal reflecting layer resulting in loss of clarity of the fringe pattern image.

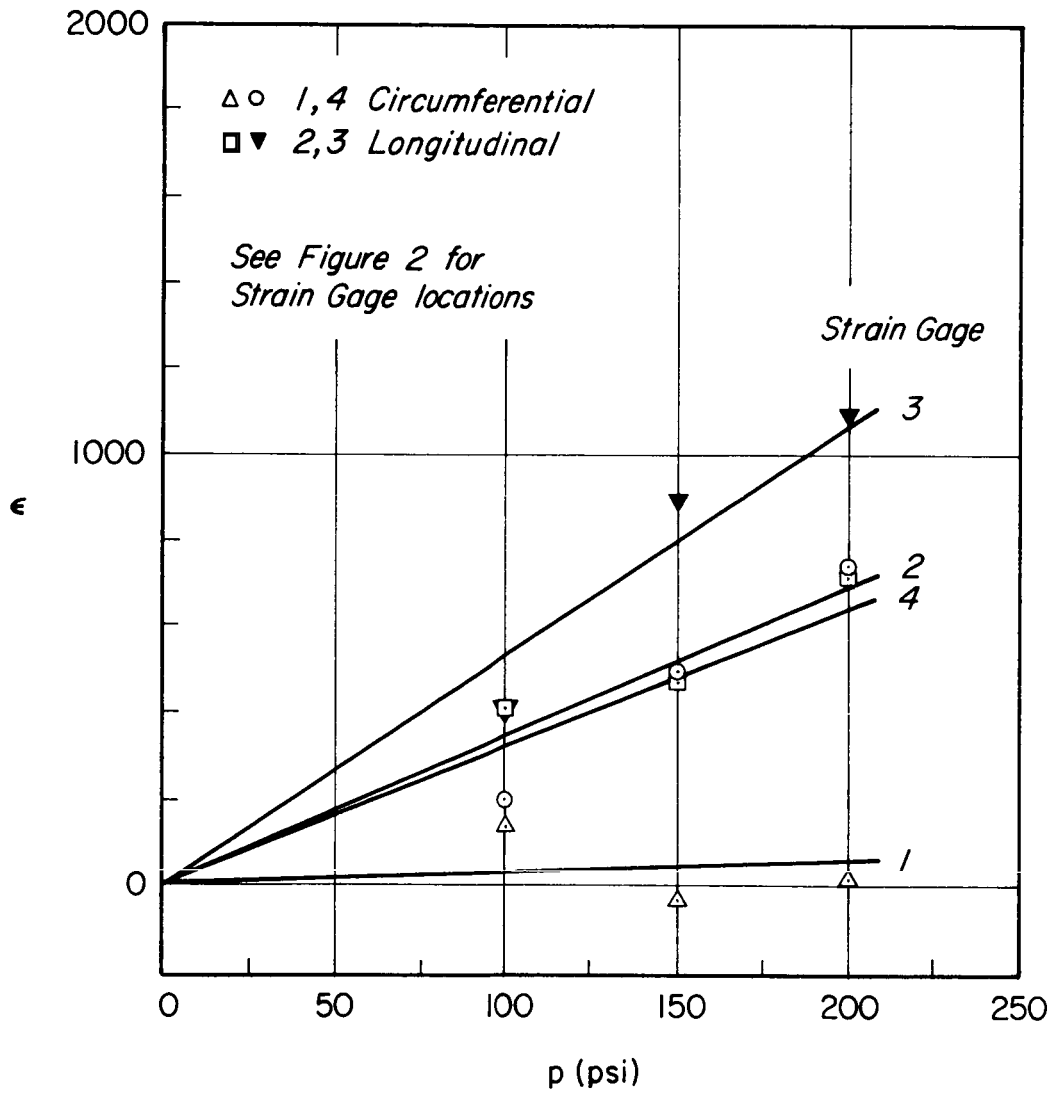


Figure 4 Strain Gage Data for 3D Model Under Pressure

The fringe pattern in the forward circumferential polariscope indicated a fringe order change of approximately $1/2$ between 0 psi and 100 psi at the interior location shown in Fig. 5B. This is considerably less than the peak value which occurred at the inner boundary (not visible in the throat circumferential polariscope). However, the fringe order at the location shown in Fig. 5B permits a valid comparison with theory, and consequently the peak value is not required.

B. Temperature

The experimentally determined temperatures at the locations shown in Fig. 3 appear in Figs. 6 and 7 at 6 minutes after insertion of the chilling fluid for two successive runs. The two sets of data indicate the reproducibility of the experiment. The temperature contours, obtained from plotting these data, are shown in Fig. 8.

The experimental thermoelastic data for 6 minutes after fluid insertion appear in Table 3 in terms of observed fringe order at the two circumferential polariscopes and in the longitudinal polariscope at the region of the outermost portion of the entrance cone.

Table 3 Thermoelastic Data 6 Minutes After Fluid Insertion

Location	Fringe Order
Longitudinal Polariscope, Entrance Cone	About $1/4$ to $1/2$
Throat Circumferential Polariscope, Throat Surface	$3-1/2$
Downstream Circumferential Polariscope	
a. Throat Surface	$2-1/2$
b. 0.2 Thickness Outward	$1-1/2$
c. $1/3$ Thickness Outward	$1/2$

The fringe locations were identified with the aid of the markings placed on the bonded polariscopes for this purpose.

The photoelastic fringe patterns in the skirt longitudinal polariscope appear in Fig. 9. The maximum fringe order (at 6 minutes after insertion of the chilling fluid) is $2-1/2$, which is a reduction from the peak of $4-1/2$ observed at 1 minute. The expected character of a bending stress field is evident at 6 minutes, whereas the inward crowding at earlier times is indicative of the earlier stage of the transient.

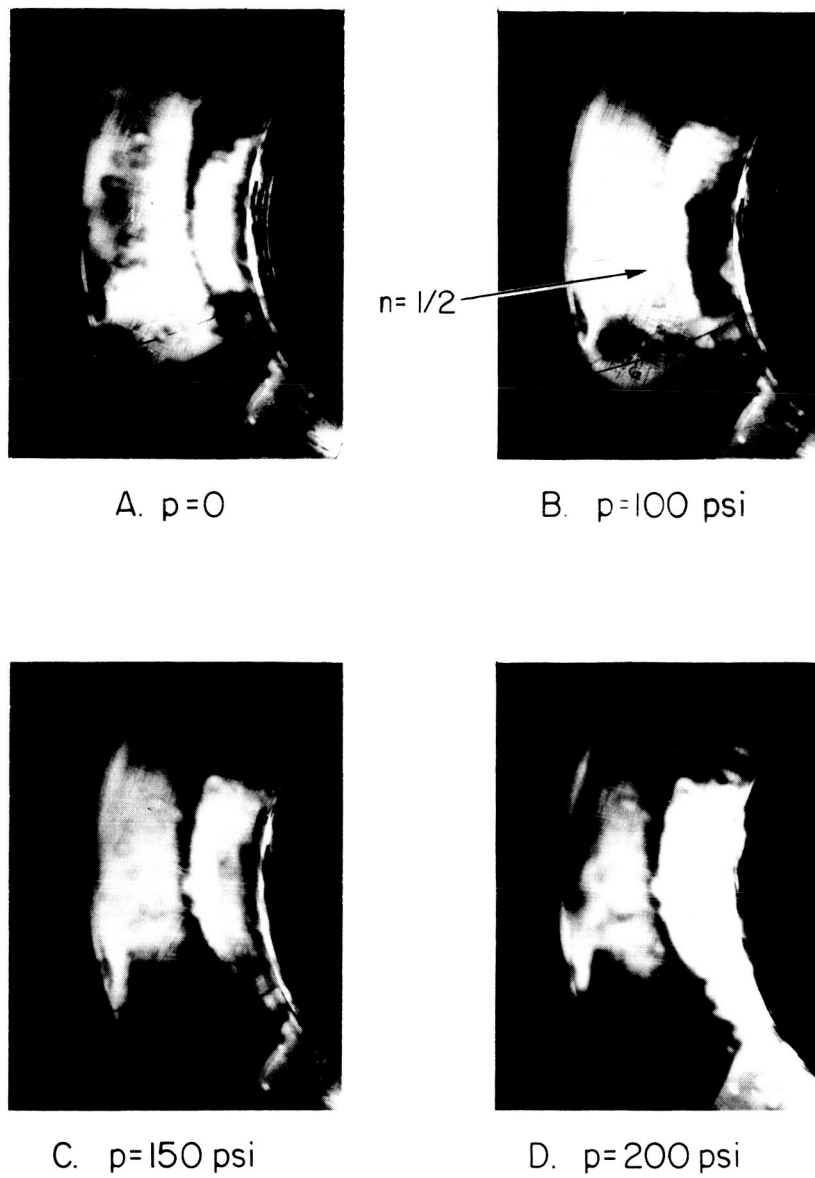


Figure 5 Fringes in Forward Circumferential Polariscope

Thermo- couple Position Galv. #1	T (F)	Thermo- couple Position Galv. #2	T (F)
ice	32.2	ice	32.0
1	39.6	9	36.3
2	57.1	10	55.4
3	64.0	11	65.6
4	66.4	12	69.5
5	33.3	13	34.2
6	53.0	14	62.6
7	63.6	15	68.7
8	66.2	16	67.1
ice	31.8	ice	32.2
17	32.6	21	39.6
18	59.5	22	47.9
19	63.4	23	60.9
20	63.0	24	65.8
25	31.8	28	29.6
26	40.0	29	33.5
27	45.5	30	35.3

Figure 6 Thermal Test - 6 Minute Data - First Run

Thermo- couple Position Galv. #1	T (F)	Thermo- couple Position Galv. #2	T (F)
ice	32.5	ice	32.2
1	43.1	9	38.6
2	59.3	10	57.1
3	66.9	11	67.8
4	70.1	12	70.4
5	35.4	13	36.4
6	55.6	14	64.0
7	66.7	15	69.6
8	70.3	16	69.7
ice	32.1	ice	32.3
17	35.5	21	42.3
18	62.5	22	50.9
19	66.1	23	62.8
20	66.2	24	68.3
25	34.3	28	32.3
26	42.6	29	36.1
27	47.8	30	37.4

Figure 7 Thermal Test - 6 Minute Data - Second Run

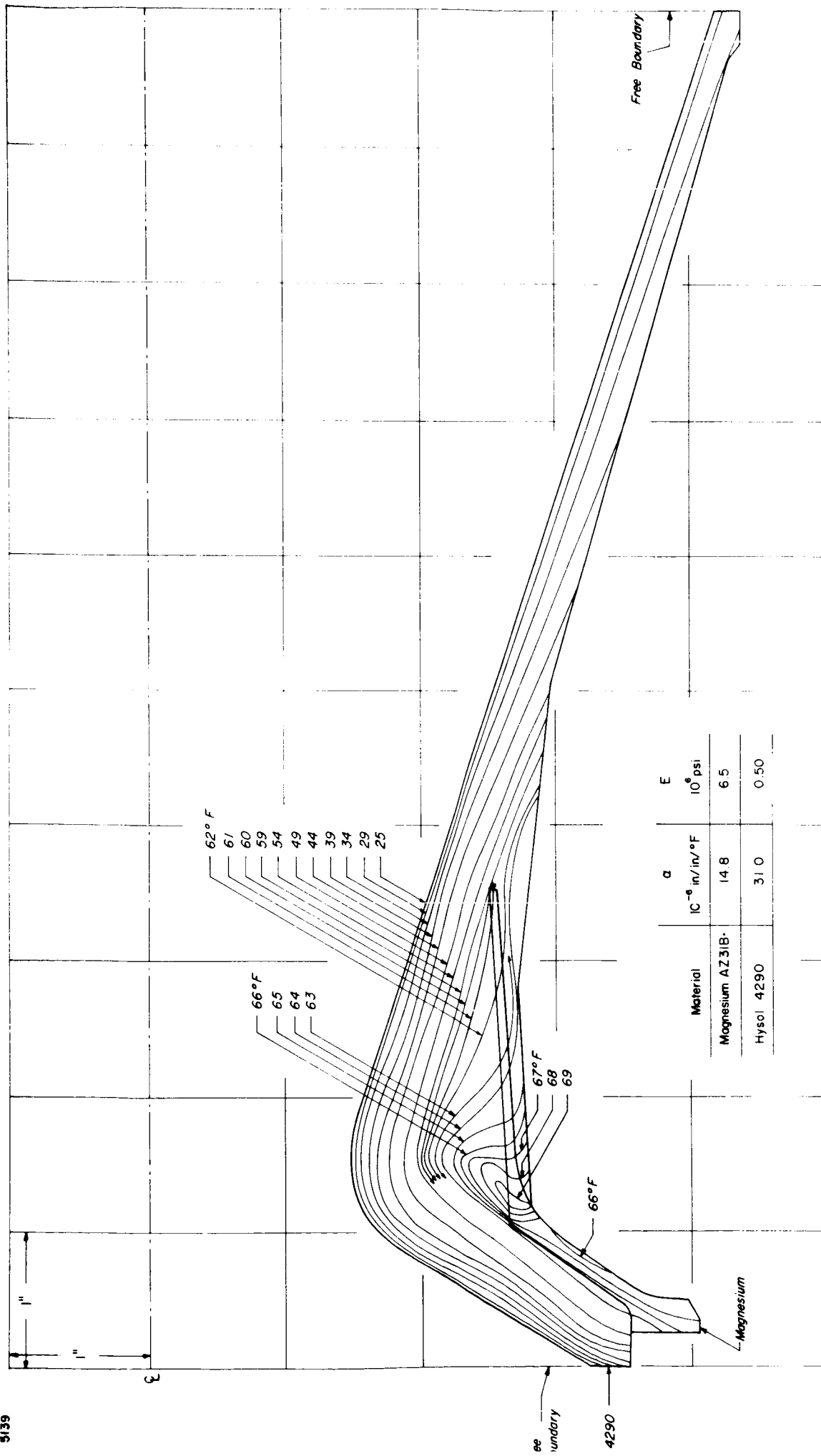
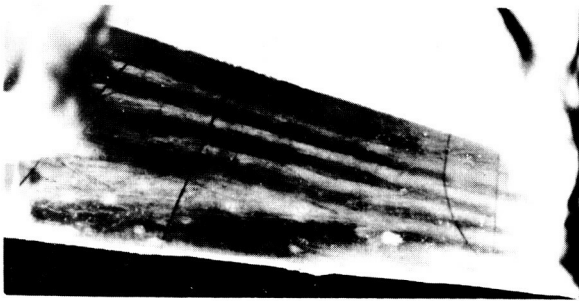
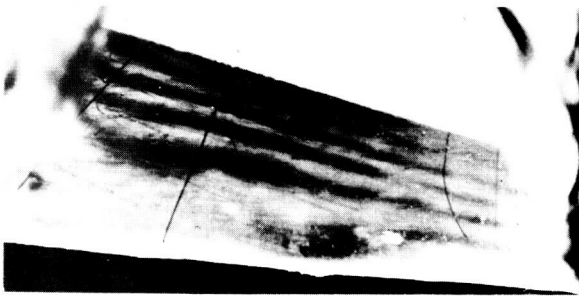


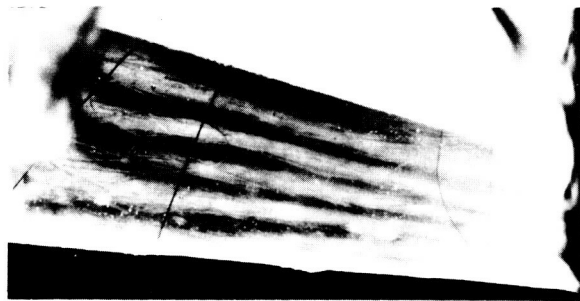
Figure 8 Photoelastic Model Temperatures for Algol II-B Thermal Test
Time - 6 minutes



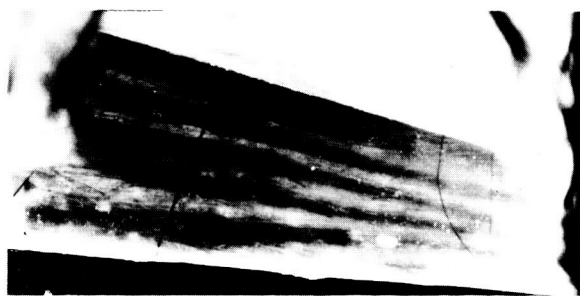
T = 0 min



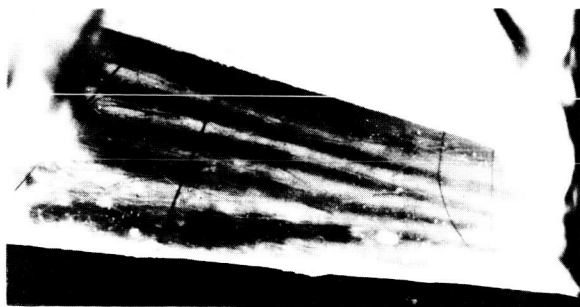
T = 1 min



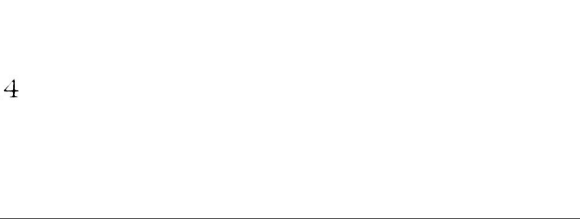
T = 2 min



T = 3 min



T = 4 min



T = 6 min

Figure 9 Fringe Patterns in the Skirt Longitudinal Polariscope

2.3 Theoretical Analysis

A. Introduction

A subcontract was let to the Research Division of Aerojet General at Sacramento (AGC) to conduct separate computer analyses of stresses in the modified ARA 3D model (Fig. 1) under inlet pressure and a selected temperature distribution. Pressure stresses were computed for both longitudinal restraint and for total restraint (clamped) at the nozzle flange bolt circle. In addition, the stresses due to a ring moment at the bolt circle were computed for longitudinal restraint. Upon completion of the calculations, AGC plotted (p - q) contours on the longitudinal cross-section. A brief report (reproduced in Appendix I directly from the original) summarized their method. The results are also available on the computer printouts, two sets of which were sent to ARA.

B. Pressure

The region of pressurization was identified in Fig. 1. This corresponds to the pressurized zone in the hydrostatic tests conducted on the prototype nozzle. The computation network and node points for the analysis are shown in Fig. 10. The results of the unit pressure analysis appear as the (p - q) contours shown in Fig. 11 for longitudinal restraint and in Fig. 12 for a clamped bolt circle. The curves delineate the localization of the stress field in the neighborhood of the inlet and throat, with rapid decay beyond the throat.

The nozzle inlet stress field is seen to build up to a peak bending stress in the region of the throat in the case of longitudinal restraint (Fig. 11). Because of the uncertain nature of the restraint in the 3-dimensional model at the time of inception of the subcontract to AGC, the additional result of (p - q) contours for a ring moment loading was obtained (Fig. 13).

The computer printout also permitted determination by ARA of the stresses on the magnesium alloy surface at the locations of the strain gages.

Table 4 Stresses on the Surface of the Magnesium Alloy Reinforcement

Strain Gage Pair	Nearest AGC Computer Element	Circumferential σ_{θ}/p	Longitudinal σ_{x}/p
(1, 2)	51	13	29
(3, 4)	83	24	36

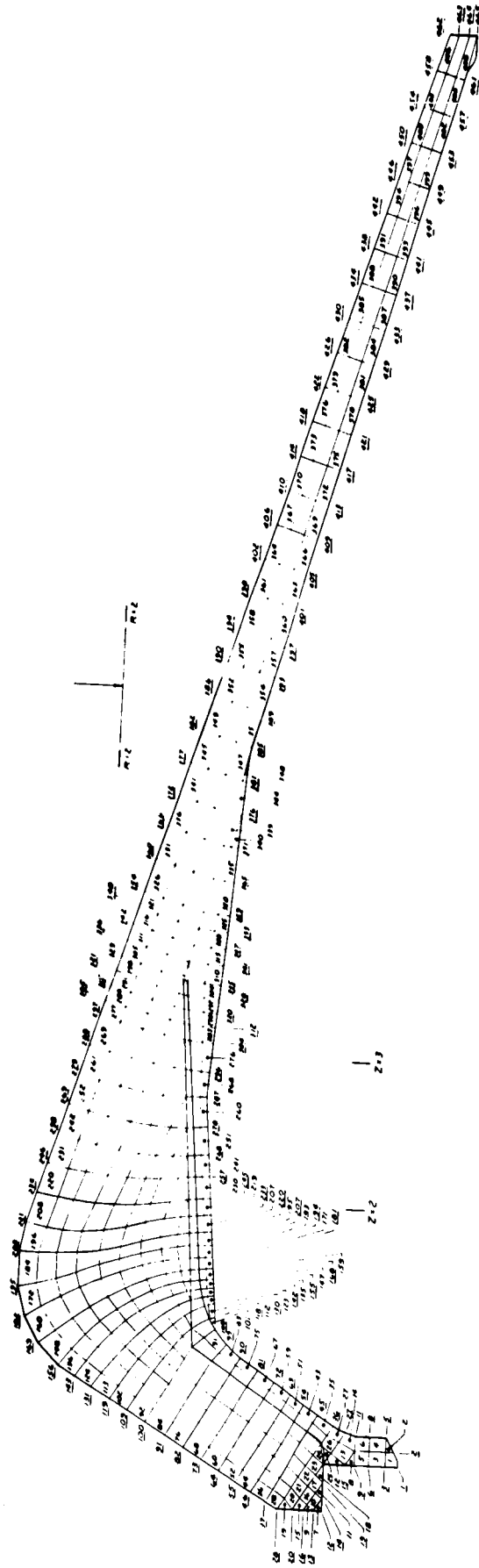


Figure 10 Algol II-B Photoelastic Model
Finite Element Representation Showing Element and Nodal
Point Numbers

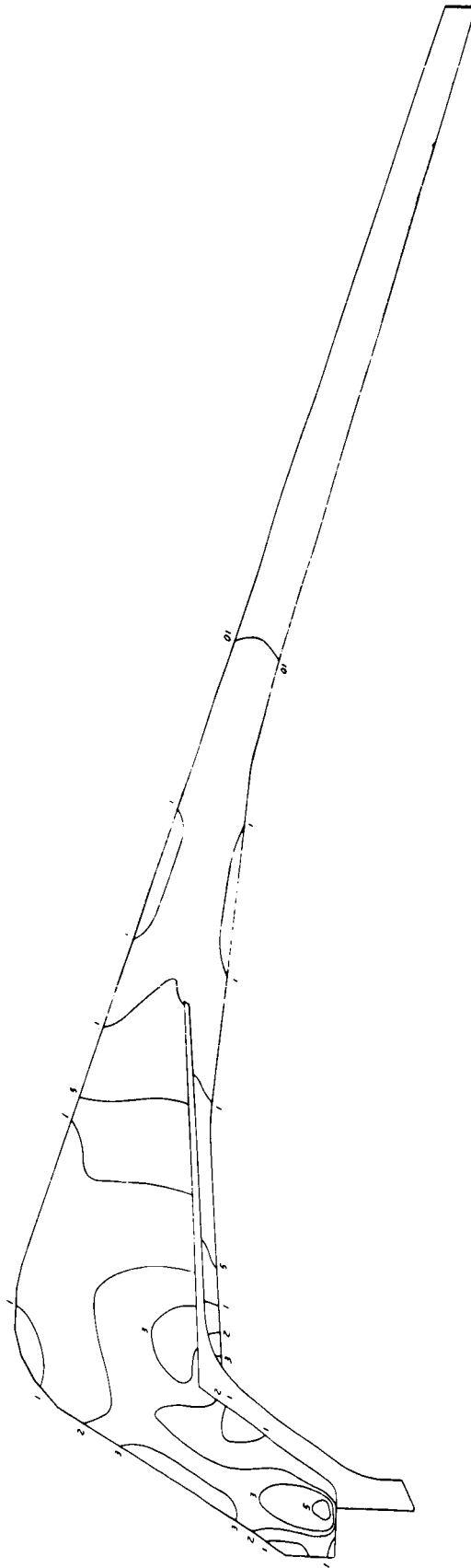


Figure 11 Contours of Principal Stress Differences, psi
Unit Pressure Loading Simply Supported at Bolt Circle

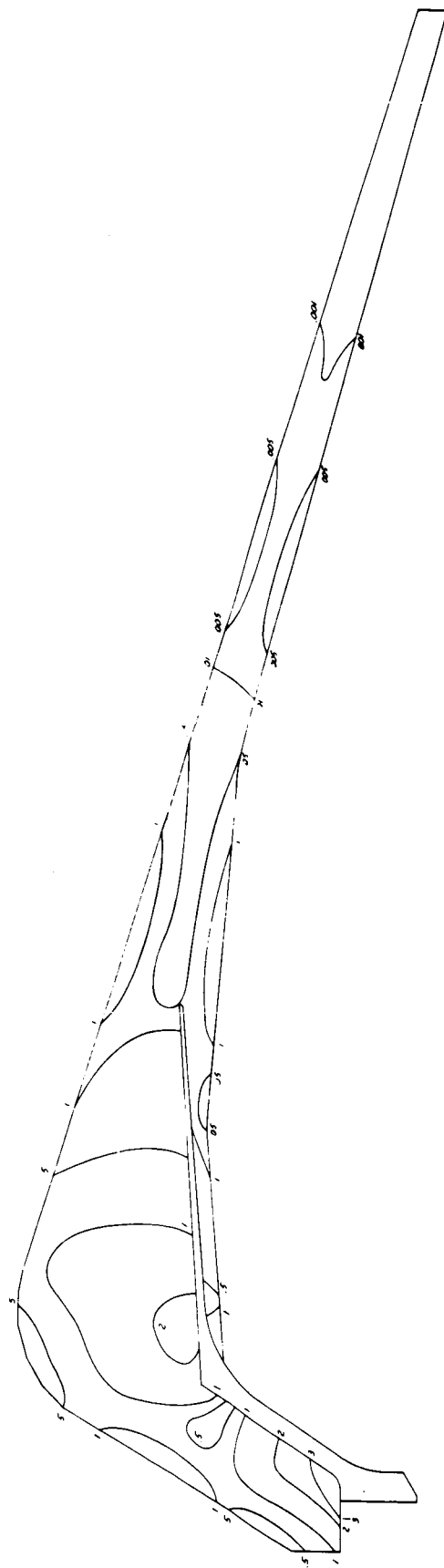


Figure 12 Contours of Principal Stress Differences, psi
Unit Pressure Loading Clamped at Bolt Circle

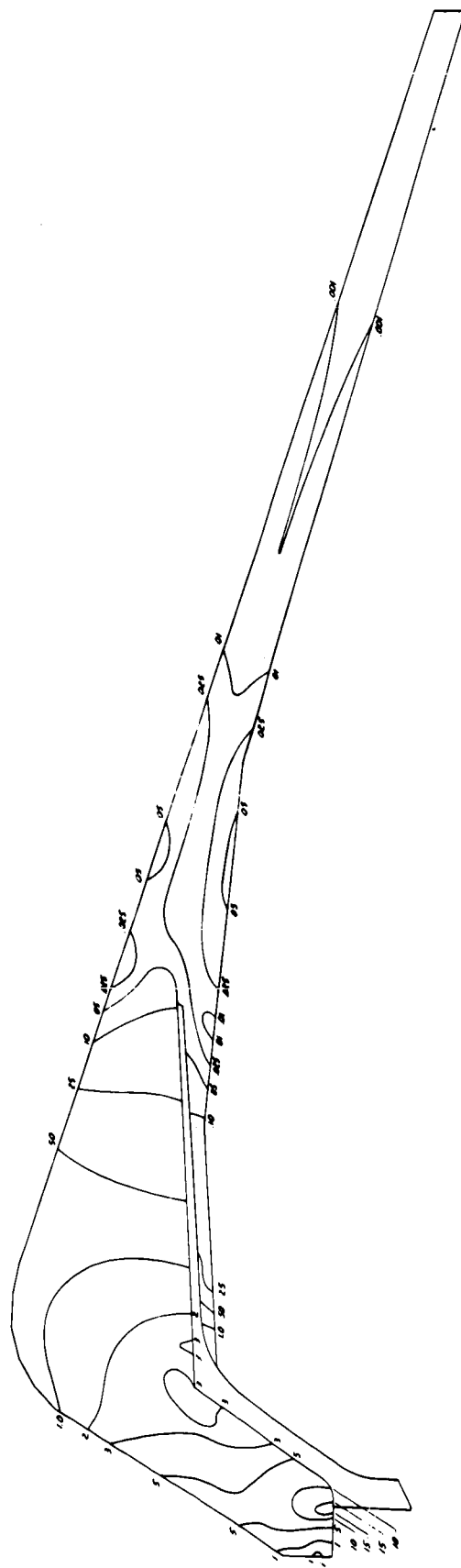


Figure 13 Contours of Principal Stress Differences, psi
Unit Ring Moment at Bolt Circle Simply Supported

The results were obtained by linear extrapolation to the surface from the interior elements in the reinforcement.

The calculations of theoretical fringe orders to be expected in the two circumferential bonded polariscopes under pressure loading appear in Table 5.

C. Temperature

The temperature distribution chosen for the computer analysis is the 6-minute field for which experimental data from the 3-dimensional model are discussed in Section 2.2 B. The general character of a beam bending stress field predominates throughout virtually the entire nozzle, as is seen in the (p - q) contours displayed in Fig. 14. The radially non-linear variation over the cross-section in the throat region clearly reflects the transient character of the temperature field shown in Fig. 8.

The data for the regions of the circumferential polariscopes were obtained from information in the AGC computer printout. Calculations for these regions are shown in Table 6.

Table 5 Theoretical Fringe Orders in Circumferential
Polariscopes, 100 psi Pressure Loading

($t = 1/4$ in., $f = 54$ psi-in/fringe, and $f/t = 216$ psi/fringe)

(1) Longitudinally Supported

Forward Polariscopes				
Analysis Element	σ_{θ}	σ_r	$\sigma_{\theta} - \sigma_r$	$\frac{(\sigma_{\theta} - \sigma_r) t}{f} = n$
172	+ 97.1	- 94.2	+191.3	0.89
173	+ 98.1	- 50.4	+148.5	0.69
162	+ 89.4	- 12.5	+101.9	0.47
163	+ 98.0	+ 26.6	+ 71.4	0.33
152	+109.3	+ 71.6	+ 37.7	0.17
153	+130.7	+100.2	+ 30.5	0.14
142	+161.4	+142.3	+ 19.1	0.09
143	+180.9	+140.0	+ 40.9	0.19
Aft Polariscopes				
291	+ 34.7	- 0.5	+ 35.2	0.16
299	+ 29.3	- 1.0	+ 30.3	0.14
300	+ 27.5	- 2.8	+ 30.3	0.14
308	+ 24.8	neg	+ 24.8	0.11
309	+ 21.8	- 1.6	+ 23.4	0.11
310	+ 19.5	- 0.6	+ 20.1	0.09

(2) Clamped

Forward Polariscopes				
Analysis Element	σ_{θ}	σ_r	$\sigma_{\theta} - \sigma_r$	$\frac{(\sigma_{\theta} - \sigma_r) t}{f} = n$
172	+115.5	- 93.7	+209.2	0.97
173	+111.2	- 56.8	+168.0	0.78
162	+102.2	- 26.5	+128.7	0.60
163	+102.5	- 2.6	+105.1	0.49
152	+106.7	+ 33.2	+ 73.5	0.34
153	+116.0	+ 54.3	+ 61.7	0.29
142	+133.1	+ 83.0	+ 50.1	0.23
143	+143.5	+ 84.0	+ 59.5	0.28
Aft Polariscopes				
291	+ 22.5	+ 0.6	+ 21.9	0.10
299	+ 17.2	+ 0.1	+ 17.1	0.12
300	+ 15.2	- 1.0	+ 16.2	0.12
308	+ 12.4	+ 1.9	+ 10.3	0.05

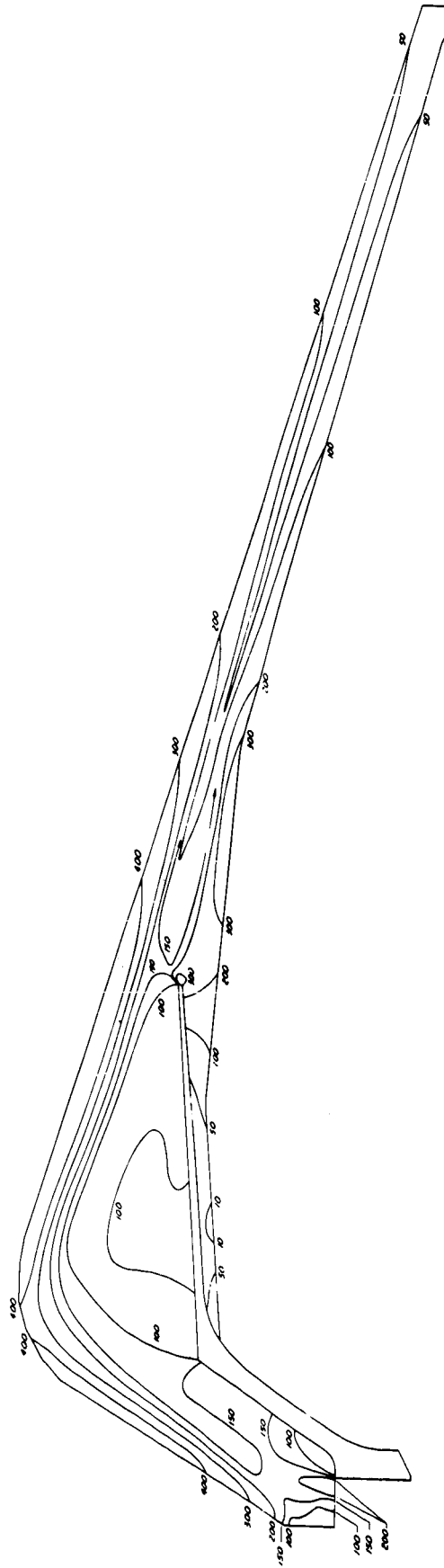


Figure 14 Contours of Principal Stress Differences, psi
 Thermal Condition at Time - 6 Minutes
 Simply Supported at Bolt Circle

2.4 Comparison of Theory and Experiment

A. Pressure

Experimental and theoretical reinforcement stresses are compared in Table 7.

Table 7 Theory and Experiment Compared on Magnesium Reinforcement

Strain Gage	Nearest Computer Element	Experimental Data		Computer Theory		Ref. 2 Analysis	
		σ_{θ}/p	σ_{ℓ}/p	σ_{θ}/p	σ_{ℓ}/p	σ_{θ}/p	σ_{ℓ}/p
(1, 2)	51	10	25	13	29	24	41
(3, 4)	83	34	44	24	36	23	54

Reasonably good agreement is seen at (1, 2), which is on the longitudinally flat portion of the reinforcement. The greater difference between computer theory and specimen at (3, 4) may be the result of a slight stress concentration, since the gages were in the region of the fillet. The computer analysis readout did not contain sufficient data to permit precise extrapolation because of the choice of elements.

The disagreement with the results of Ref. 2 is apparent, and this disagreement is magnified for stresses in the interior which are considerably lower than the magnesium surface, whereas Ref. 2 indicated stresses there of the same order as shown in Table 7.

The fringe order observed in the longitudinal polariscope was considerably lower than deduced from the AGC computer program. This is traceable to the indistinct character of the fringe pattern. A possibly higher fringe order appeared to be present but was not reliably identifiable.

A photoelastic datum obtained from the forward circumferential polariscope is compared to the theoretical curve in Fig. 15, which shows reasonable agreement for 100 psi applied pressure. (The fringe order was estimated to be within 1/8 fringe of the correct value.)

B. Temperature

The theoretical values of principal stress difference in the region of the longitudinal polariscope near the throat inlet are shown to be of the order of 100 to 150 psi, where the plastic was cemented to the magnesium shell. This corresponds

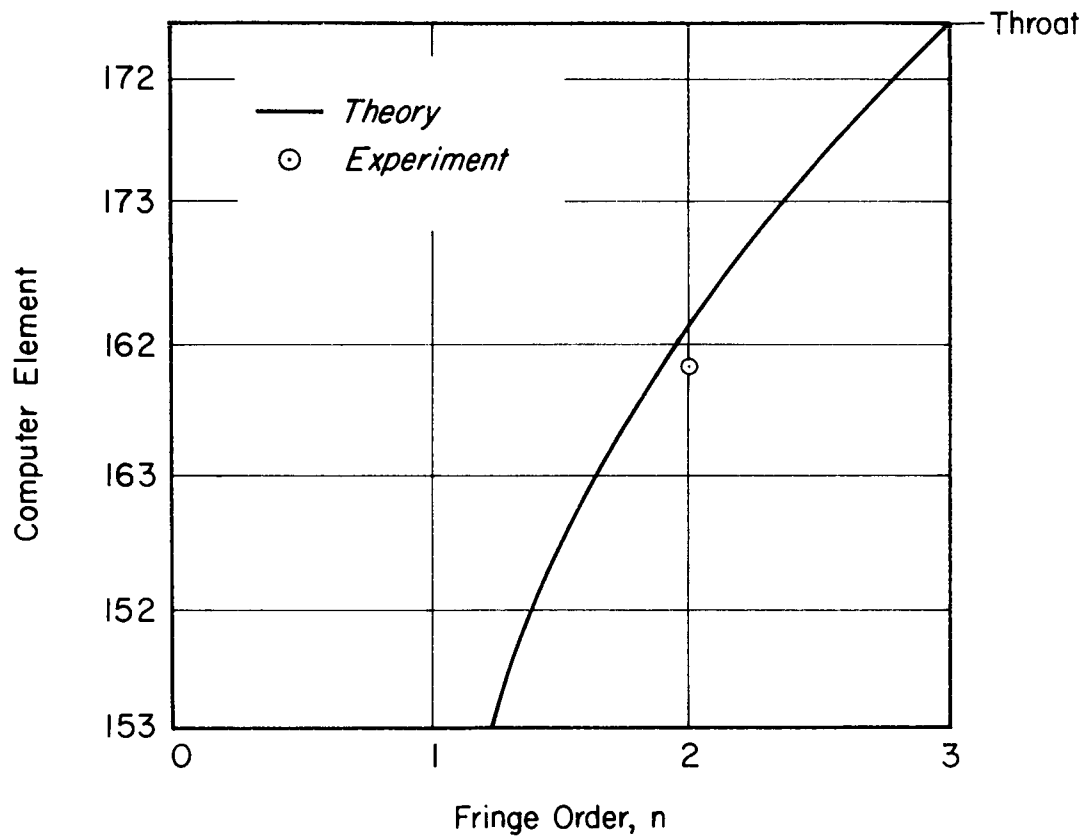


Figure 15 Comparison of Theory and Experiment For 100 psi. Pressure At Forward Polariscope

to 1/2 to 0.7 fringes since 1 fringe was equivalent to 216 psi. This corresponds in general to the value of 1/4 to 1/2 reported in Table 1.

The theoretical radial fringe order distributions in the two circumferential polariscopes were computed from σ_{θ} and σ_r as shown in Table 6 in the region of the model in which fringes were observable in the bonded polariscopes. The agreement with the experimental data appears in Fig. 16.

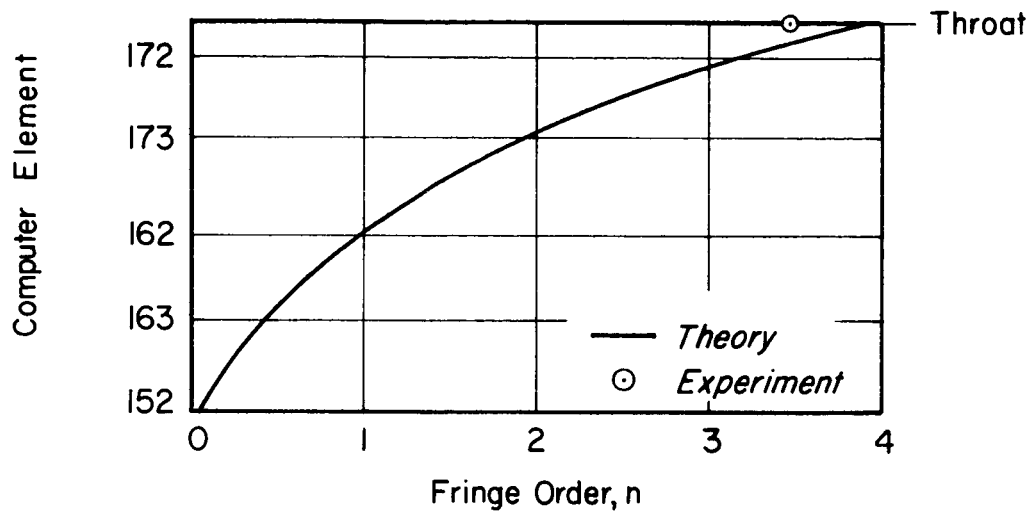
The longitudinal data in the skirt polariscope at 6 minutes were compared to the theoretical values shown in Fig. 14, using 216 psi = 1 fringe. The general characters of the fields agree well, as do the peak values, although there are some differences in details possibly resulting from the magnesium reinforcement which has a sharp edge at that location.

C. Pure Moment Loading

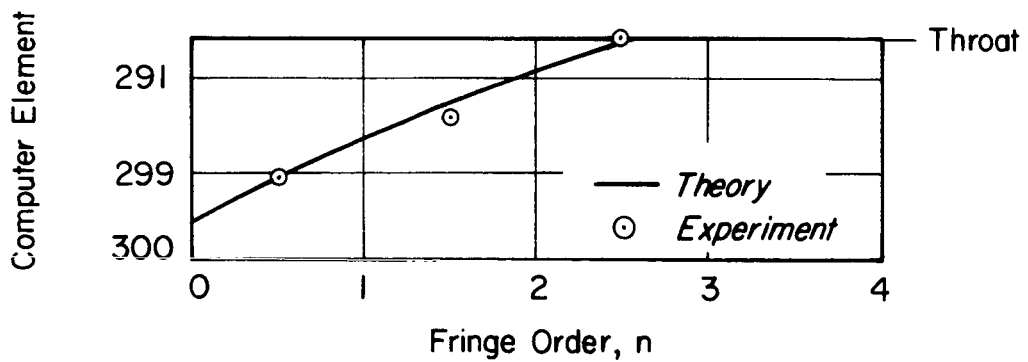
The sharp decay of local loading is evident in Fig. 13 which differs radically from the continuous moment distribution on the 2D beam (Ref. 1, Fig. 5) based on the principal stress differences computed theoretically by AGC for the ring moment loading. Vanishingly low stresses are to be anticipated aft of the throat section in the 3D nozzle in contrast to the continuous 2D distribution, as is to be expected.

D. Summary

In spite of the moderate precision of the fringe order data (1/4 fringe in 3, or 8 percent error) resulting from the model complexities, fabrication difficulties, and problems in reading the polariscopes, there is little doubt that theory and experiment are essentially in agreement for both pressure and temperature loadings. The theoretical and experimentally observed low stress levels substantiate the observations reported in Ref. 1 which, at that time, were contrary to the predictions of the design stress analysis (Ref. 2).



a.) FORWARD POLARISCOPE



b.) AFT POLARISCOPE

Figure 16 Comparison of Theory and Experiment For Temperature Loading

3. ELASTIC FOUNDATION MODEL STUDY

3.1 Introduction

The use of three dimensional photoelasticity sometimes may not be completely effective in providing solutions to stress analysis problems in complex structures such as the Algol II-B rocket nozzle. Furthermore, if a variety of loading conditions require investigation, such a procedure could be time consuming and costly. For the same reasons, such approaches may be undesirable during design. On the other hand, the general picture of stresses in a structure available from photoelasticity makes it desirable to employ this general technique for such structural problems. This section of the project describes an investigation of a procedure which offered the possibility of solving these problems. It is based upon employment of two dimensional models in which are incorporated the feature which provides three dimensional behavior to a body of revolution.

An axisymmetric shell under axisymmetric loading may be considered to behave structurally as a series of longitudinal beams supported by an elastic foundation. This model has been successful in analyzing circular cylindrical shells under mechanical and thermal loads. If a photoelastic beam simulating the shell longitudinal section were to be supported by an appropriate planar photoelastic foundation, the longitudinal and circumferential stresses in the shell should be revealed. Furthermore, it would have the advantage of determining stresses throughout the shell for unit loading at any longitudinal location, thereby permitting assessment of a variety of loading conditions by simple summation. In addition, design changes could be incorporated in the model with relatively little difficulty and cost.

The remainder of this part of the report is devoted to a detailed description of the development and application of this new photoelastic technique to analysis of the Algol II-B rocket nozzle under internal pressure loading in the entrance and throat region.

3.2 Preliminary Studies

A. Purpose

Once the concept of the elastic foundation photoelastic model is put into words, it is almost evident that the approach should work. However, the step between a concept and practice sometimes is large. Consequently, it was considered important to conduct an elementary experiment before attempting the construction of the elastic foundation model of the Algol II-B nozzle. This preliminary investigation was intended to reveal possible limitations to the method and difficulties of model fabrication, as well as a check on the accuracy of the procedure, before proceeding with the Algol II-B simulation,

The subject chosen for this preliminary investigation was a uniform wall circular cylinder loaded by edge shears and moments. The following sections depict the basic elastic foundation theory, describe the model, and show the agreement of theory and experiment for this simple case.

B. Theory

The basic elastic foundation relation for an axisymmetric isotropic shell under axisymmetric loading is shown in Fig. 17. From equilibrium of radial forces and longitudinal moments

$$\frac{\partial V}{\partial x} = \bar{p}, \quad \frac{\partial M}{\partial x} = V \quad (1)$$

Therefore

$$\frac{\partial^2 M}{\partial x^2} = \bar{p} \quad (2)$$

where \bar{p} is an equivalent pressure loading arising from the elastic foundation effect produced by the circumferential ring forces. In terms of material properties, shell geometry and radial deformation,

$$\bar{p} = -(Et/R^2) w \quad (3)$$

since outward motion induces inward pressure. Therefore

$$\frac{\partial^2 M}{\partial x^2} + \frac{Et}{R^2} w = 0 \quad (4)$$

The foundation modulus, Et/R^2 , is the radial stiffness of the ring of length dx acting to restrain the dx beam segment. If a planar foundation is constructed with this same stiffness, then a longitudinal strip of shell which is supported

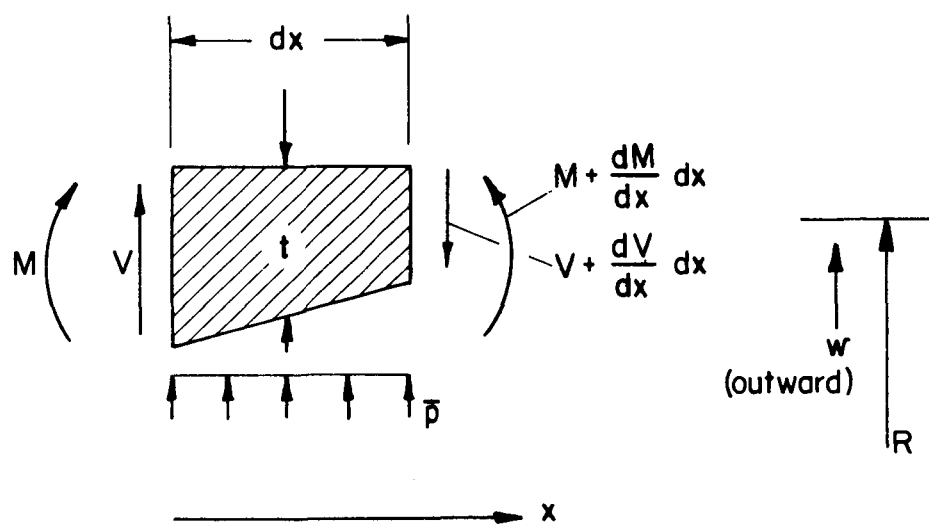


Figure 17 Cross Section of Length dx of Shell Wall

by that foundation should behave structurally in the same manner as in the actual shell. If the longitudinal centerline of the shell is selected as a rigid reference for the foundation, then (Fig. 18)

$$\frac{pR^2}{E_1 h} = w = \frac{PL}{AE_2} \quad (5)$$

using elementary strut theory. This relation reduces to an expression for the length of the foundation column,

$$L = \frac{t_2 W_2}{t_1 W_1} \frac{R^2}{h} \frac{E_2}{E_1} \quad (6)$$

If a large range of foundation materials is available so that E_2/E_1 may be selected at will, then it is most convenient to have $t_1 = t_2$ and $W_1 = W_2$, so that

$$L = (R^2/h) (E_2/E_1) \quad (7)$$

which involves only the shell local radius and radially measured thickness. The choice of W ($=W_1 = W_2$) then becomes a matter of model design which may reflect other considerations to be discussed in the following section.

C. Experimental Procedure

In theory, the elastic foundation should consist of infinitely many parallel springs of zero x extent and finite stiffness. In practice they would consist of parallel columns of finite W . The first portion of this preliminary experimental investigation was to determine the importance of W upon proper foundation behavior. For this purpose a pair of epoxy beams was cemented to a urethane slab (Fig. 19) as a first approximation to the proper design and was loaded as shown in Fig. 20. The rigid center reference line was obtained from symmetry.

Upon reduction of the data, differences between theory and experiment indicated that as a second approximation the foundation behavior could be improved by slitting as shown in Fig. 19. After this modification the model was retested with satisfactory results.

D. Comparison of Theory and Experiment

The experimental data are revealed in the fringe patterns of Fig. 21 and are compared to theory (Ref. 4) in Fig. 22. There was good agreement even for the

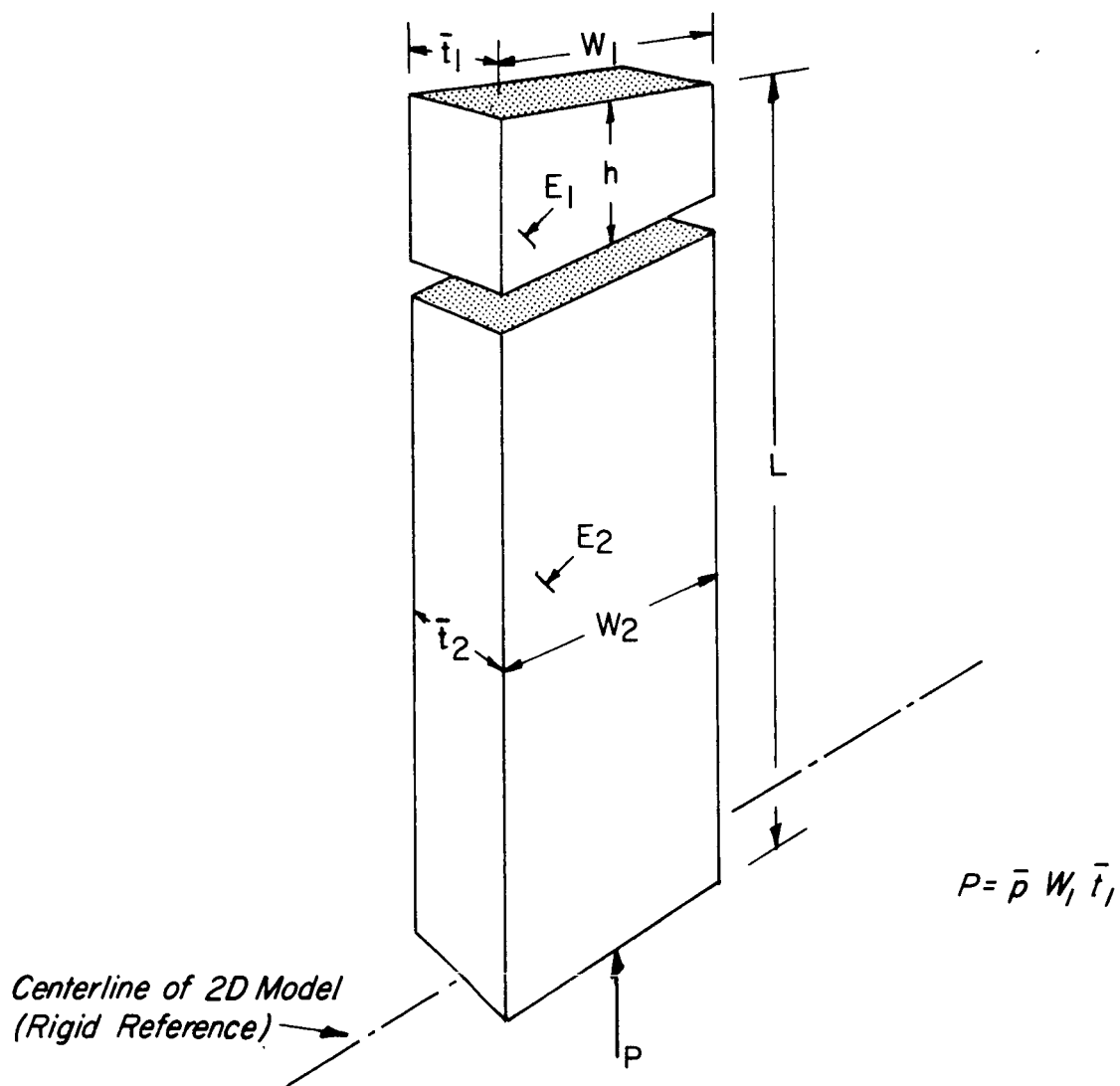
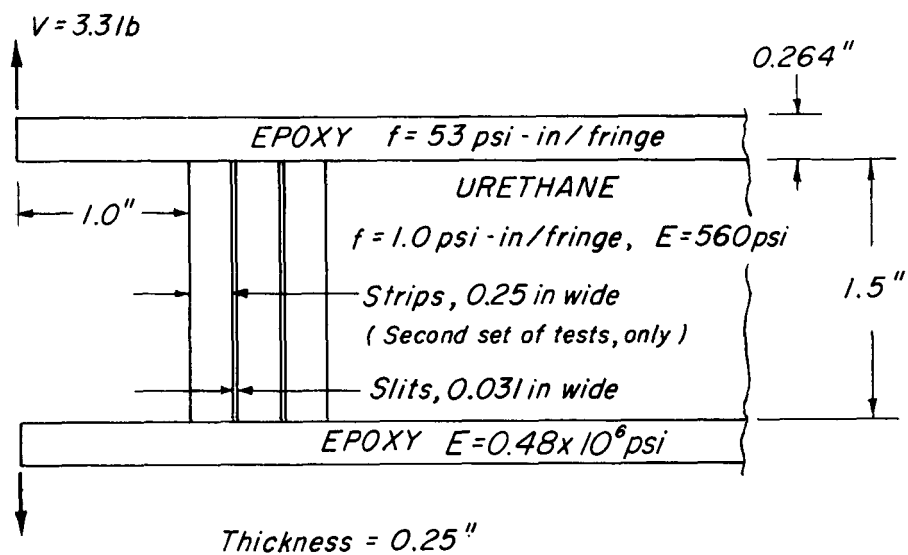


Figure 18 Elastic Foundation Column Geometry



Corresponds to Epoxy Circular Cylindrical Shell with $R = 12.9$ and with Same Wall as Epoxy Beams.

Figure 19 Model Geometry and Material Properties

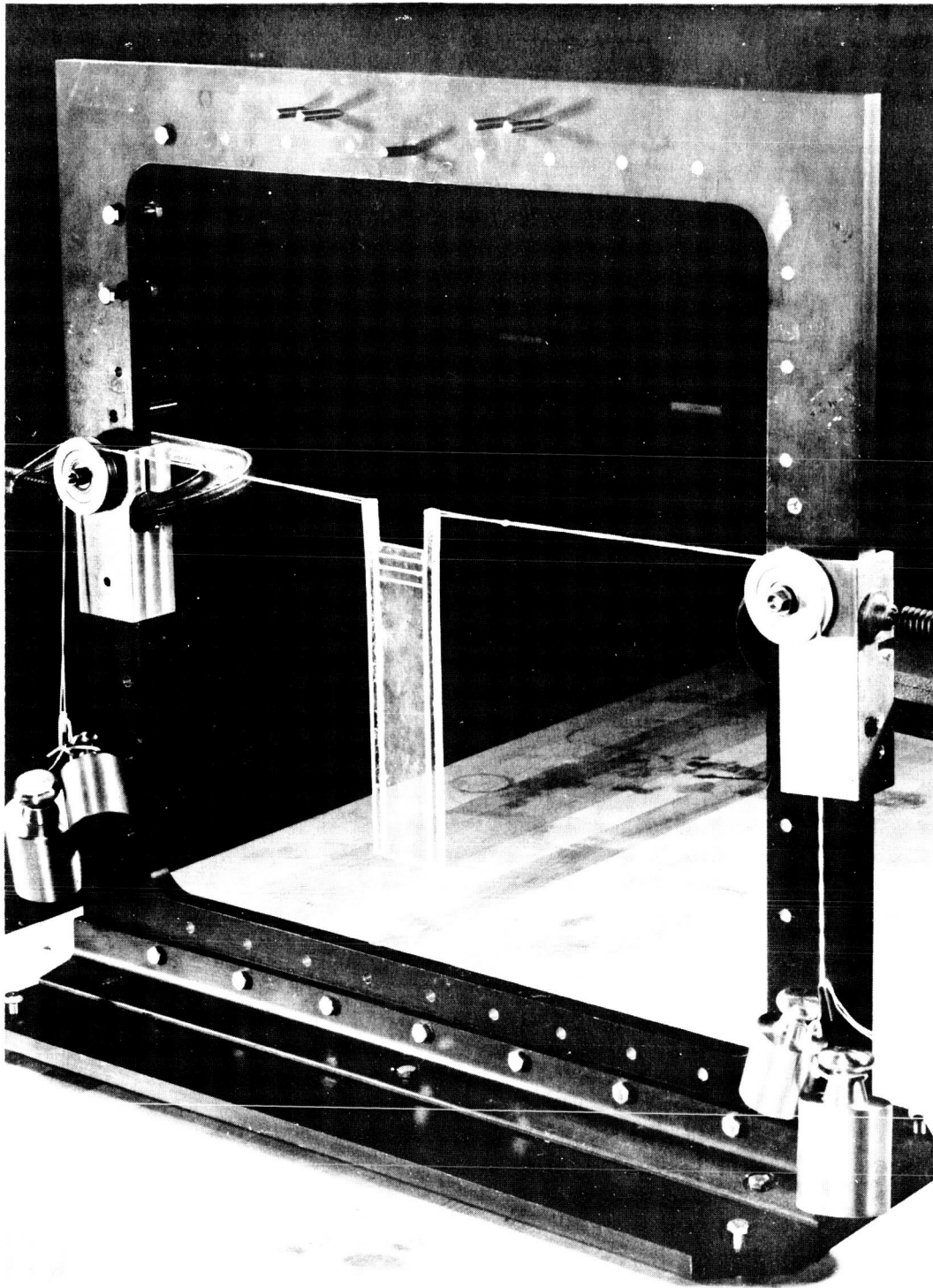
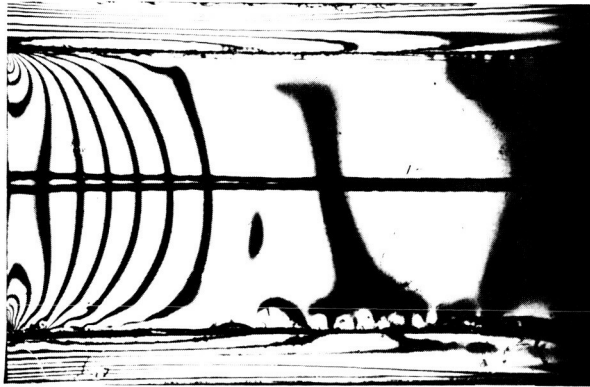
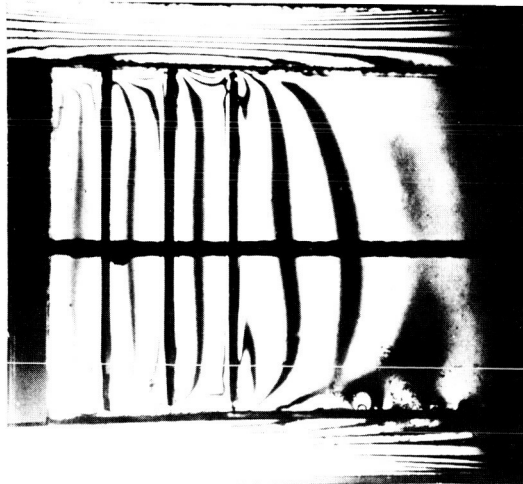


Fig. 20 Experimental Arrangement for Preliminary Tests on Beam - on - Elastic - Foundation Model



A. Uncut Slab Foundation



B. Foundation With 3 Strips and Slab

Fig. 21 Fringe Patterns in Elastic Foundation Photoelastic Models

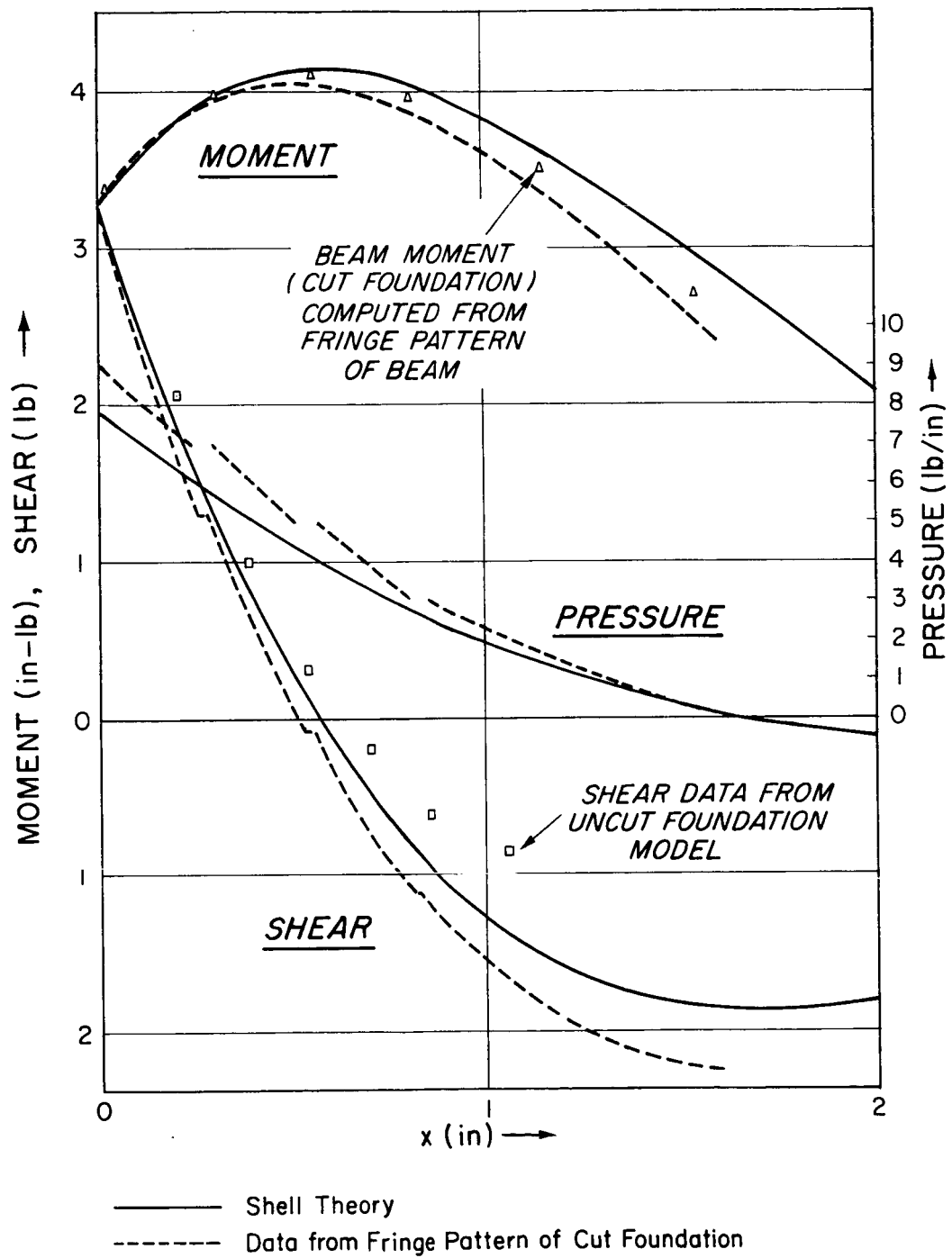


Figure 22 Correlation of Theory and Experiment for Preliminary Elastic Foundation Studies

relatively coarse approximations to the exact foundation. The broken character of the shear and pressure lines reflect the linear x variation in foundation reaction across the width of each strip as a result of bending instead of a curved variation to match the longitudinal epoxy beams.

The pressure was determined at the longitudinal centerline of the model directly from the stress optic law. This curve was integrated once to obtain the dashed line shear diagram and again to obtain the dashed line moment curve.

At this stage the validity of the approach was considered reasonably well established, and it was decided to proceed directly to the elastic foundation model of the three dimensional Algol II-B nozzle model.

3.3 Algol II-B Simulation

A. Model Design

The elastic foundation simulation of the Algol II-B three dimensional model is depicted in Fig. 23, which portrays the photoelastic arrangement and loading system. The model dimensions appear in Fig. 24. Fabrication of the longitudinal beams representing the nozzle cross section was obviated through the use of the two beams (1/2 prototype scale) investigated in the 2D studies described in Ref. 1.

It was necessary to construct the foundation employing the relationship shown in Eq. 6, modified to account for the thick ring behavior and composite material properties of the nozzle in the inlet and throat regions. This problem was examined in Ref. 1 in comparing longitudinal and circumferential cross section properties.

The metal structure along the model centerline was necessary to accomodate the varying lengths of the elastic foundation columns. These backup strips of aluminum alloy essentially provided stiff support and represented the rigid reference line discussed previously, since the model was constructed symmetric about the centerline between the longitudinal beams. Variations in column section, as well as changes in column material, are evident in Figs. 23 and 24. These illustrate the need for engineering design of an elastic foundation model for a three dimensional structure with the complexity of the Algol II-B nozzle.

B. Experimental Procedure

Point loads were applied to the model at the locations shown in Fig. 25. Strong cord was employed for this purpose since it provided a most efficient means of controlling force and direction through use of dead weights and pulleys, as shown in Fig. 23. The cords permitted determination of stresses in the region of major stress level under a radial edge load of 25 lb. applied 2.4 in. above the entrance cone of the 1/2 scale model to produce a moment of 60 in-lb., and under rings of pressure in the entrance cone and throat. Fringes were photographed under radial edge and moment loading. However, fringe orders under pressure ring loading were less than 1 fringe and consequently were measured at each data station (Fig. 25) with a Babinet compensator. The effect of inlet pressure was obtained by integration of the pressure ring data at each data station of the model.

This process of reduction of the pressure stresses was tedious since it was necessary to align the compensator parallel to the principal stress direction at each data point. Furthermore, errors were introduced because of uncertainty in the

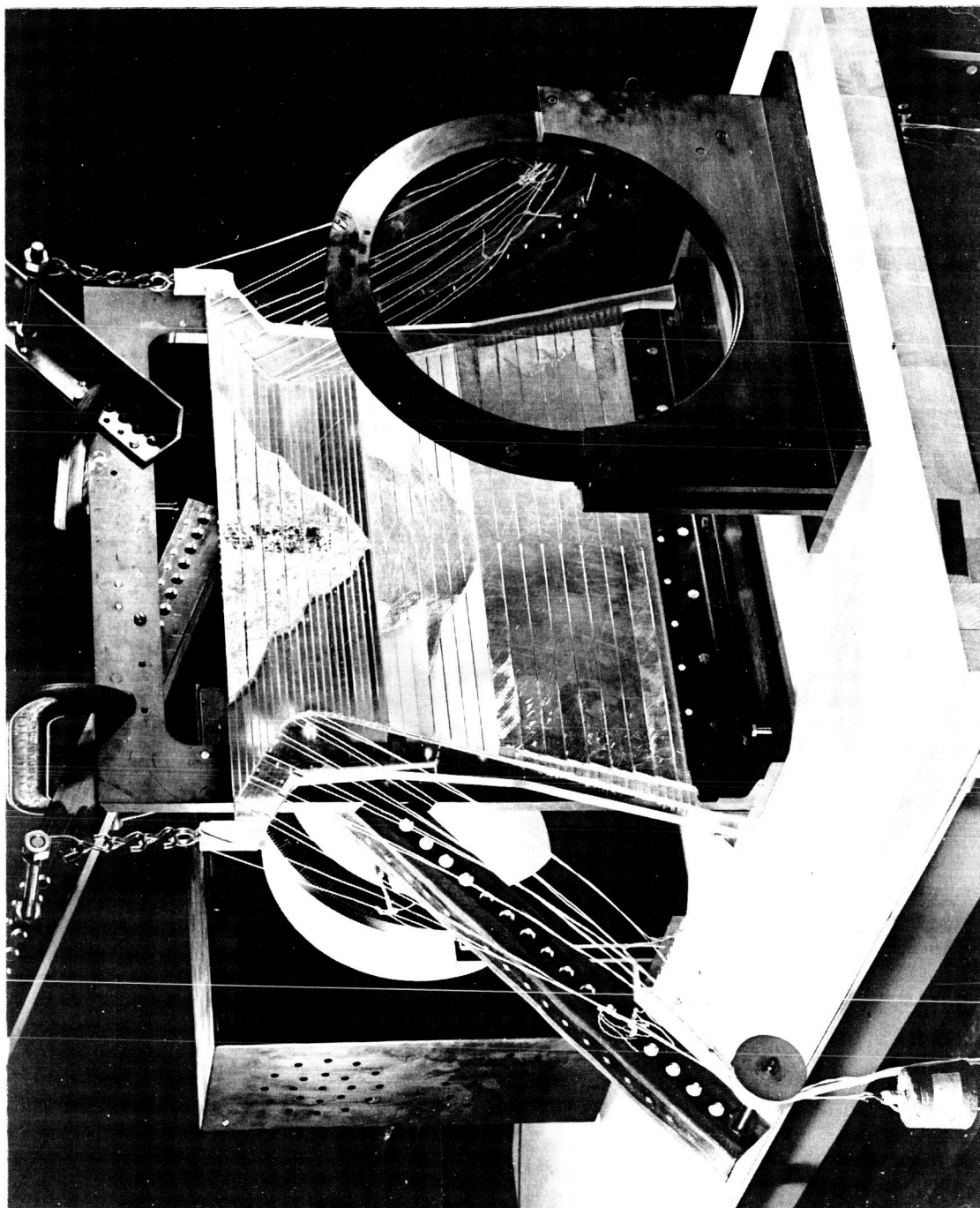


Figure 23 Elastic Foundation Model and Experimental Arrangement

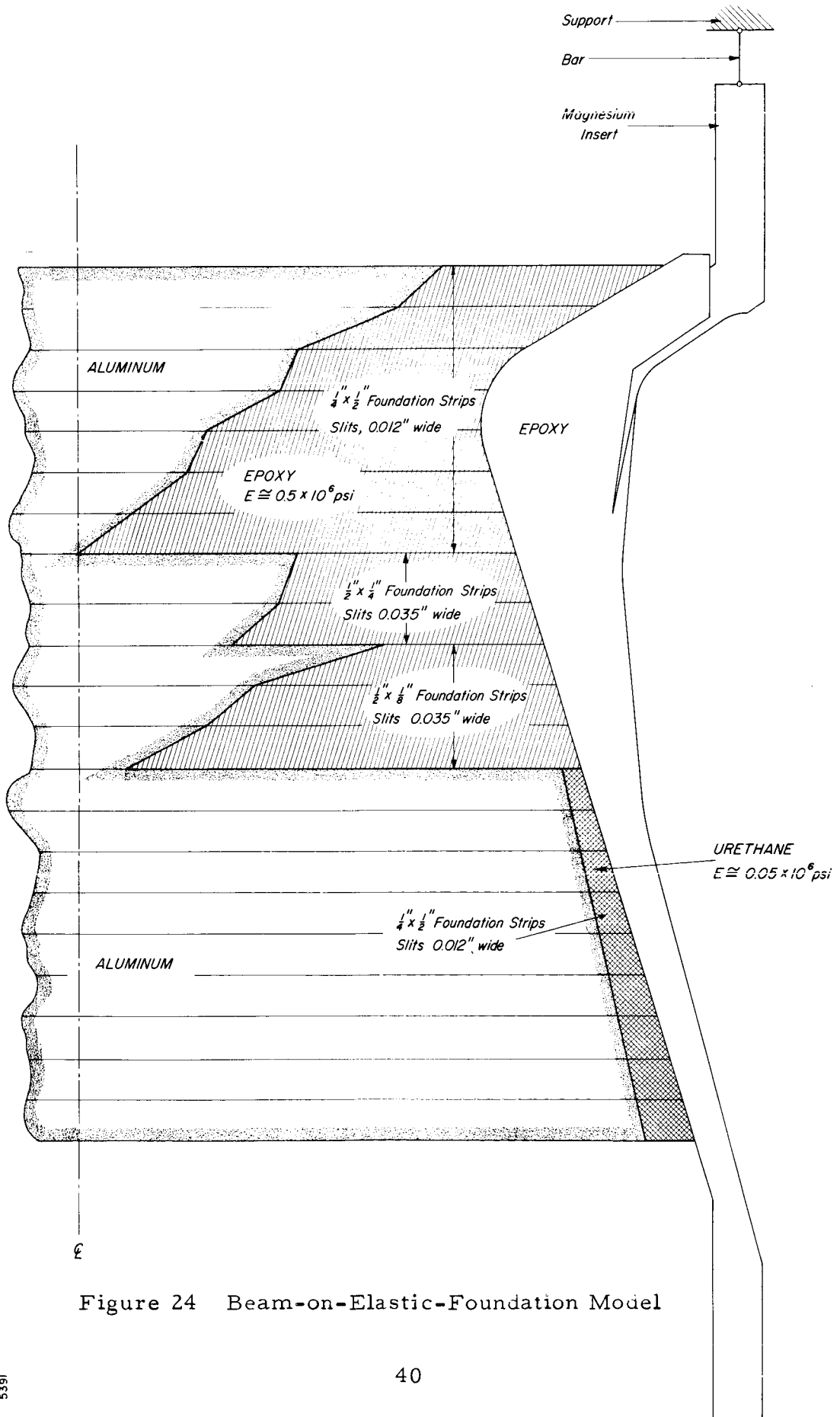


Figure 24 Beam-on-Elastic-Foundation Model

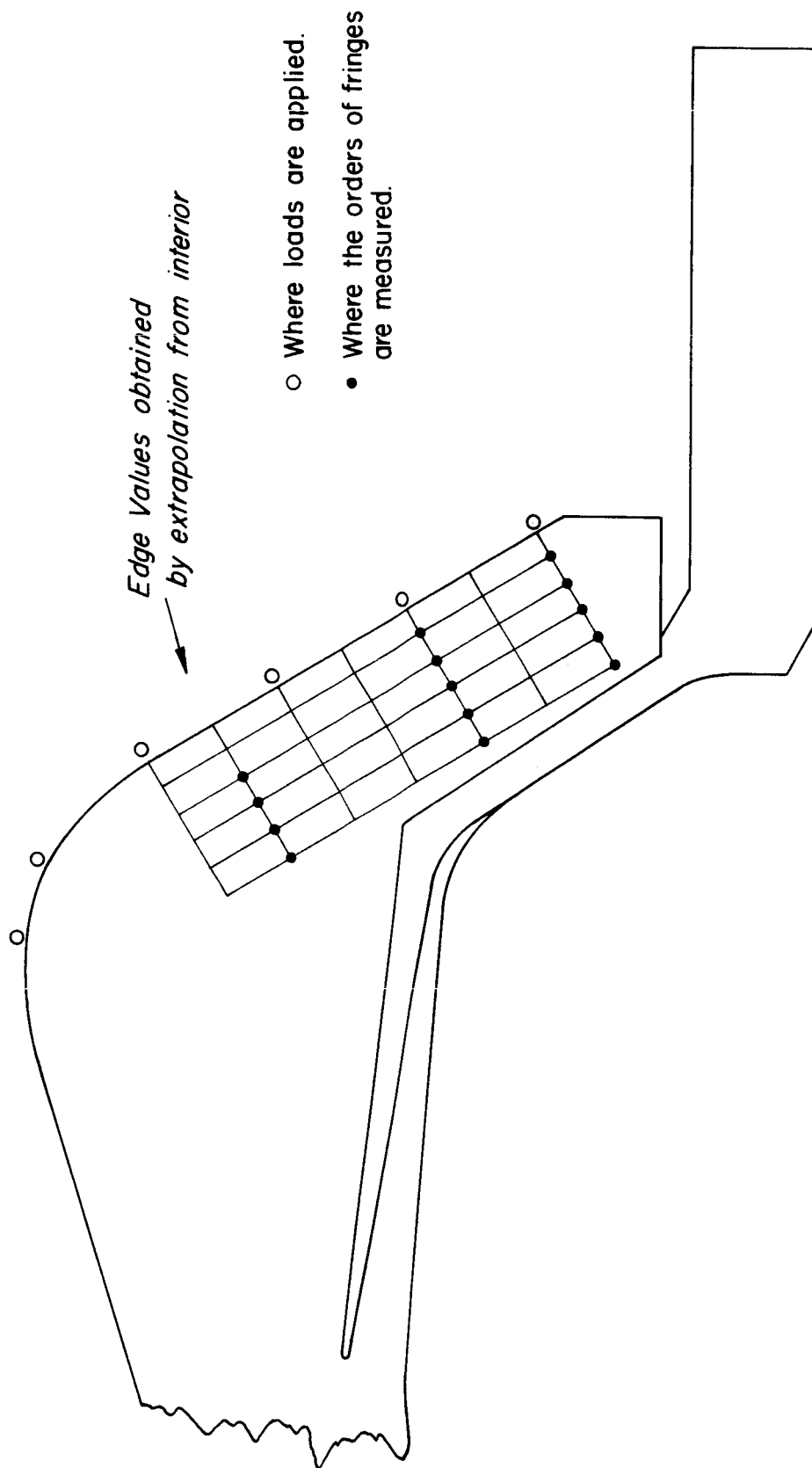


Figure 25 Data Point Locations

isoclinic angle. Finally, the integration of the influence line data to obtain fringe orders due to pressure acting over region A (Fig. 1) required consideration of the isoclinic angle at each point for the unit load at each position. This resulted in buildup of error at certain locations, as the data show.

C. Comparison With 3D Data

The AGC computer pressure analysis was conducted for both a longitudinally restrained and a clamped boundary. The ARA 3D experimental boundary condition was not controlled, and could not be measured in the experimental arrangement employed. However, it appears reasonable to assume absence of rotational restraint as evidenced by the leakage observed during that test, and consequently the assumption of a longitudinally restrained bolt circle seems reasonable for that case also. The elastic foundation model was supported longitudinally only. Therefore the pressure data for these three situations should be in agreement.

The agreement of the data for the 3D model with theory was demonstrated in Section 2.4A. As may be seen in the comparison of Fig. 26, the theoretical fringe pattern agrees well with the data for the elastic foundation model under pressure, although it differs in some areas from the values obtained at the indicated locations. Furthermore, for local moment there are differences also (Fig. 27). These discrepancies are traceable to indistinct isoclinics and fringes, and to loading of the throat contour of the elastic foundation model by the foundation columns. The foundation compressive stresses interact with those induced near the throat by the longitudinal compression in the plastic region of the longitudinal beams of the model. This indicates that it would have been useful, in this case, to turn the model inside out by reversing the longitudinal beams so that the throat edges faced outward away from the model centerline.

D. Summary

The utility of the elastic foundation photoelastic model approach to investigate axisymmetrically loaded shells of revolution is considered to have been demonstrated. For models of the complexity of the Algol II-B rocket nozzle, there may be problems in engineering the design of the model. One factor which could simplify this process is the availability of a variety of photoelastic materials covering a large modulus range.

The photoelastic data obtained with this model show a general similarity to the 3D results. It is felt that this agreement could have been improved by reversing

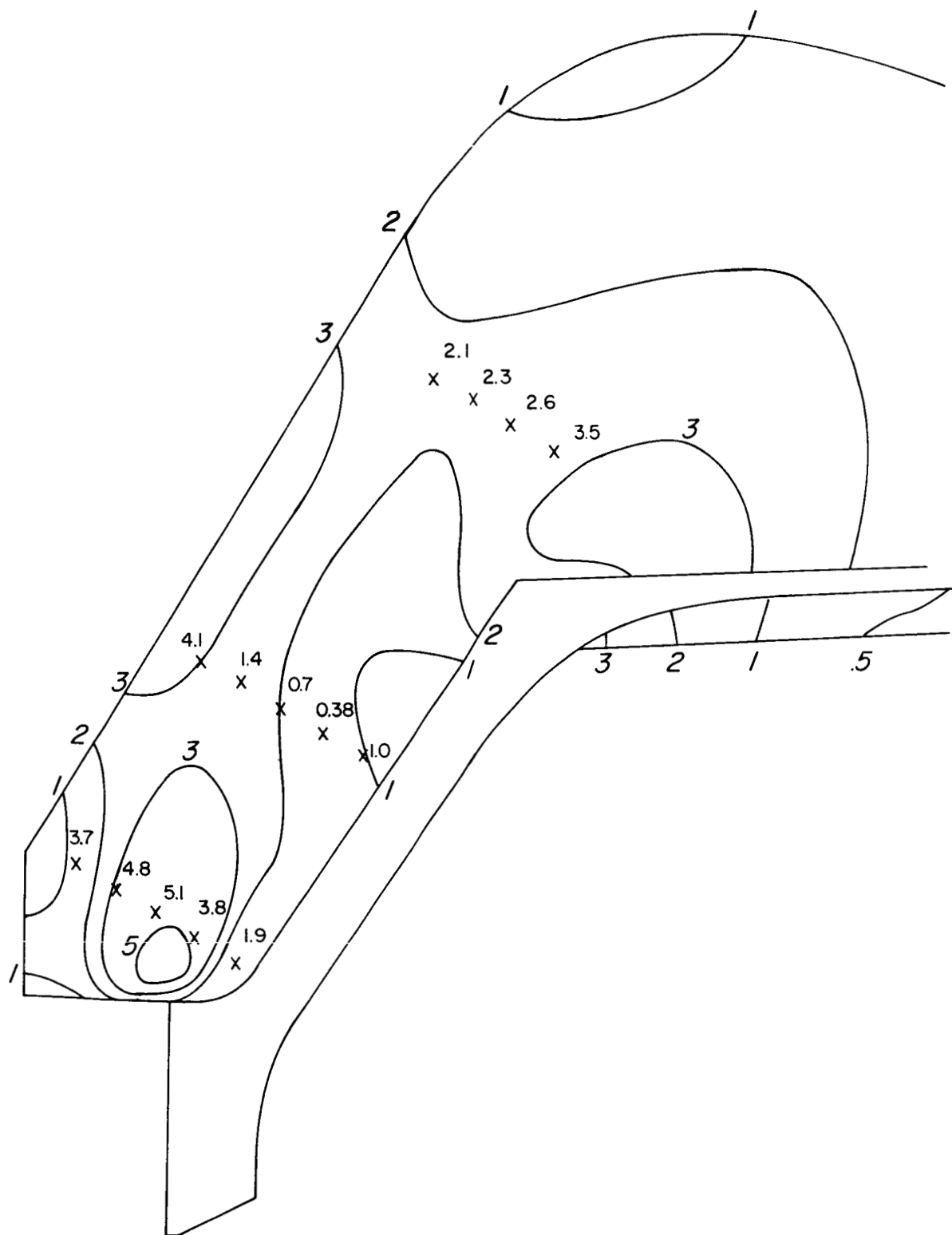
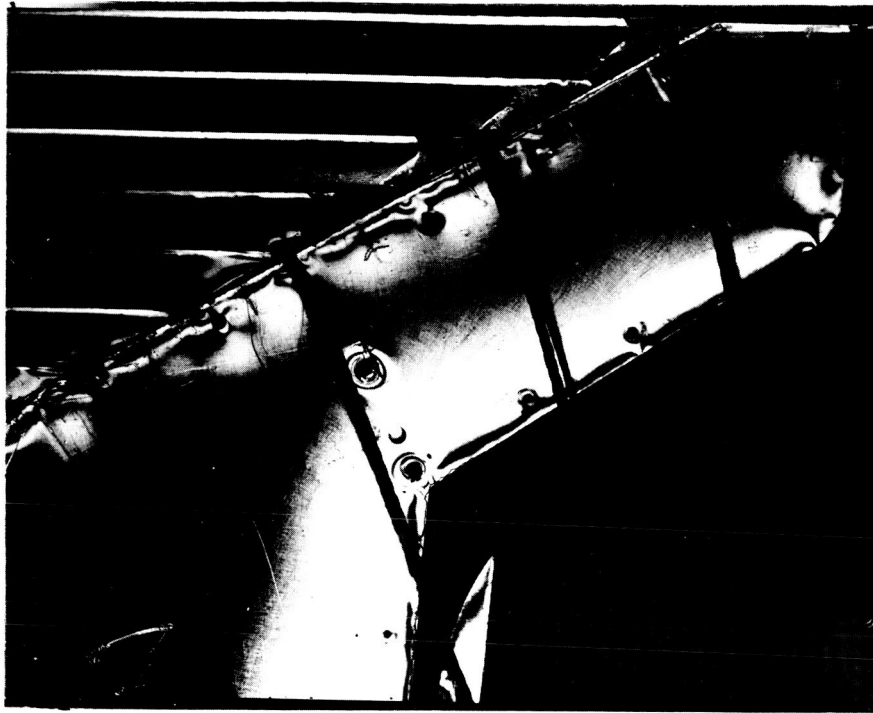


Figure 26 Comparison of Elastic Foundation Pressure Model Data With AGC Theory.



A. Before Loading



B. Radial Shear of 25lb. 2.4in. Above Top of Plastic

Figure 27 Edge Shear and Moment Loading

the orientations of the longitudinal beams which represent the cross section of the nozzle. The alteration of the beam fringe patterns by the elastic foundation forces was avoided in the preliminary cylinder model by reading fringes on the outer unloaded edges of the beams, resulting in good correlation with theory.

APPLIED RESEARCH ASSOCIATES, INC.

4. CONCLUSIONS

A. 3D Nozzle Analysis

1. Experiment and theory have been shown to agree well for a three-dimensional photoelastic model of the Algol II-B rocket nozzle loaded by pressure and by a temperature transient.
2. The results substantiate the inaccuracy in a previous theoretical stress analysis and reconfirm the low stress levels reported previously in tests conducted on the same photoelastic model.
3. The higher pressure levels employed in this investigation, together with the application of electric strain gages, were important factors in achieving the correlation of theory and experiment.

B. 2D Elastic Foundation Model

1. A demonstration has been presented of the soundness of the principle of constructing an elastic foundation for a 2D photoelastic model of the cross-section of an axisymmetric shell axisymmetrically loaded.
2. Experiments on an elastic foundation model of the 3D nozzle model yielded results in fair agreement with the 3D analyses.
3. Improvements could yield techniques which would provide greater accuracy in the data.

5. REFERENCES

1. Becker, Herbert and Hamilton, Harold, "A Photomechanical Investigation of the Algol Solid Propellant Rocket Motor Nozzle", ARA Final Report No. 274-8, May 1965.
2. Pfluger, W. D., M. L. Hodgins and R. D. Entz, "Final Stress Report on the Algol IIA Nozzle Assembly", Aerojet General Corporation, December 13, 1963.
3. Wilson, E. L., "Structural Analysis of Axisymmetric Solids", Paper 65-143, presented at the AIAA Second Aerospace Sciences Meeting, New York, N. Y., January 25-27, 1965.
4. Timoshenko, S., "Theory of Plates and Shells", McGraw-Hill Book Company Inc., 1940.

6. APPENDIX

Reproduction of AGC Summary Report on Computer Program

STRESS ANALYSIS OF ALGOL II-B PHOTOELASTIC MODEL

1. DESCRIPTION OF THE FINITE ELEMENT ANALYSIS OF SOLIDS

A. Method of Analysis

The continuous body is replaced by a system of elements or regions of triangular or quadrilateral cross sections. The system of elements is inter-connected at joints called nodal points. The method consists of solving equilibrium equations in terms of the unknown nodal point displacements, evaluating the strain field from these displacements, and finally knowing the stress-strain relations, evaluating the stress components from the strain field solution.

Displacement or stress boundary conditions can be specified at any nodal point within the system, in addition, arbitrary mechanical, thermal and acceleration loads can be prescribed. It can be shown mathematically that the method converges to the exact solution as the element size decreases, thus, any practical degree of accuracy can be attained.

B. Finite Element Idealization

Figure 1 represents a radial cross section of the photoelastic model which has been subdivided into a system of triangular and quadrilateral elements. These elements are continuous in the hoop direction (forming rings interconnected at the nodal circles). The physical model is represented by 408 elements connected at 465 nodal points. The numbers used in labeling nodal points are under-lined to distinguish them from the element numbers. The numbering system is continuous across the body after nodal point 19 and element 20.

As seen from the figure, areas where the strain gradients are expected to be high have smaller elements than those regions where changes in strain are expected to be low.

C. Interpretation of Results

The solution consists of two basic types of information. The equilibrium equations of the system are solved for the nodal point displacements. These roots are the movements of physical points in the body, displacements are positive in the directions of positive coordinate axes. Knowing the displacements and assuming the displacement field to be linear within each element, the strains and (from these) the stresses in each element can be evaluated. The resulting stress components are those at the centroid of the element.

Boundary stresses and material interface stresses are not found directly with the finite element technique because stresses are averaged over the elemental area. Boundary values are established by means of extrapolation from the interior.

2. DESCRIPTION OF THE CASES ANALYZED

Table 1 lists the case number, loading condition, and boundary conditions for the specific conditions analyzed.

Table 1

<u>Case</u>	<u>Loading Condition</u>	<u>Boundary Condition</u>
1	Thermal ⁽¹⁾	Simple Support ⁽⁴⁾
2	Ring Moment ⁽²⁾	Simple Support
3	Pressure ⁽³⁾	Simple Support
4	Pressure	Clamped ⁽⁵⁾

Notes: (1) A reference temperature of 70°F is used with the distribution supplied for the time of 6 minutes.

(2) One inch-pound per circumferential inch is applied at the bolt circle by means of surface shears acting on nodal points 9 and 11.

(3) One pound per square inch is applied normal to the boundary from nodal points 12 to 208.

(4) Nodal circle 11 is restrained against axial (z) deflection without developing radial (R) shear forces.

(5) Nodal circles 6, 8, 9, and 11 are fixed in the axial and radial directions.

The material properties used in the solution of the cases described above are listed in Table 2.

Table 2

<u>Material Property</u>	<u>Material</u>	
	<u>Hysol 4290⁽¹⁾</u>	<u>Magnesium Z31B⁽²⁾</u>
E, 10^6 psi	0.5	6.5
α , 10^{-6} in/in/ $^{\circ}$ F	31.0	14.8
ν	0.335	0.354

Notes: (1) Called material 1 in the computer solution

(2) Material 2

3. PRESENTATION OF RESULTS

A. Contour Plots

Figures 2 through 5 are plots of contours of constant principal stress differences for the cases described in Table 1. The difference in principal stresses is always a positive quantity because the maximum principle stress is the algebraic maximum. Some judgement must be used in developing the contours in areas of stress concentration such as the region around the end of the magnesium ring embedded in the Hysol material.

The contours are obtained from the solution output by interpolating between known values at the element centroids. The intersections of the stress contours and free or inter-material boundaries are found by extrapolation from the interior.

B. Computer Output

Two copies of the solution output are included with this discussion. The results are titled with the appropriate load and boundary conditions. In addition, a copy of the computer-plotted geometry is included as verification of proper coordinate input data. The same coordinates used to plot the element network is used in the solution of the stress-analysis problem.

It is worth mentioning that each of the four solutions has the same temperature distribution. Only the analysis for thermal stresses, however, has non-zero coefficients of expansion, therefore, only the latter solutions contains thermal stresses.